SCIENTIFIC REPORT

INFRARED INTERFEROMETRY, ACTIVE GALACTIC NUCLEI, YOUNG STELLAR OBJECTS, AND EVOLVED STARS

ACTIVE GALACTIC NUCLEI

Exploring the Inner Sub-Milli-Arcsecond Torus with the Keck Interferometer in the Near-Infrared

To resolve the torus region surrounding the central black hole and accretion disk at the highest spatial resolution available, we are using long-baseline interferometry in the near-infrared. Until recently, there was only one such measurement for Type 1 AGNs, the Keck interferometer measurement of the brightest Type 1 AGN NGC 4151 (Swain et al. 2003). In May 2009, however, we finally succeeded in observing 4 Type 1 AGNs with the Keck interferometer, namely NGC 4151, Mrk 231, NGC 4051, and the QSO IRAS 13349+2438 at z = 0.108. We detect high visibilities ($V^2 \sim 0.8-0.9$ at projected baseline lengths in the range of 75 to 85 m; Fig. 1a) for all four objects including NGC 4151, for which we confirm the high V^2 level measured by Swain et al. We marginally detect a decrease of V^2 with increasing baseline lengths for NGC 4151, where the decrease and absolute V^2 are well fitted with a ring model having a radius of 0.45 ± 0.04 mas (0.039 ± 0.003 pc). This matches independent radius measurements from optical-infrared reverberation that are probing the dust sublimation radius. We also find that the effective radius of the other objects, obtained using the same ring model, is either roughly equal to or slightly larger than the reverberation radius (Fig. 1b). The measurements establish a dust sublimation radius in AGN tori that is actually smaller by a factor of about three than expected from a simple calculation with standard ISM dust grains (e.g. Barvainis 1987). The small sublimation radius could be due to the possible dominance of large grains or an anisotropy of the accretion disk radiation. → Kishimoto et al. 2009a; PR 2009

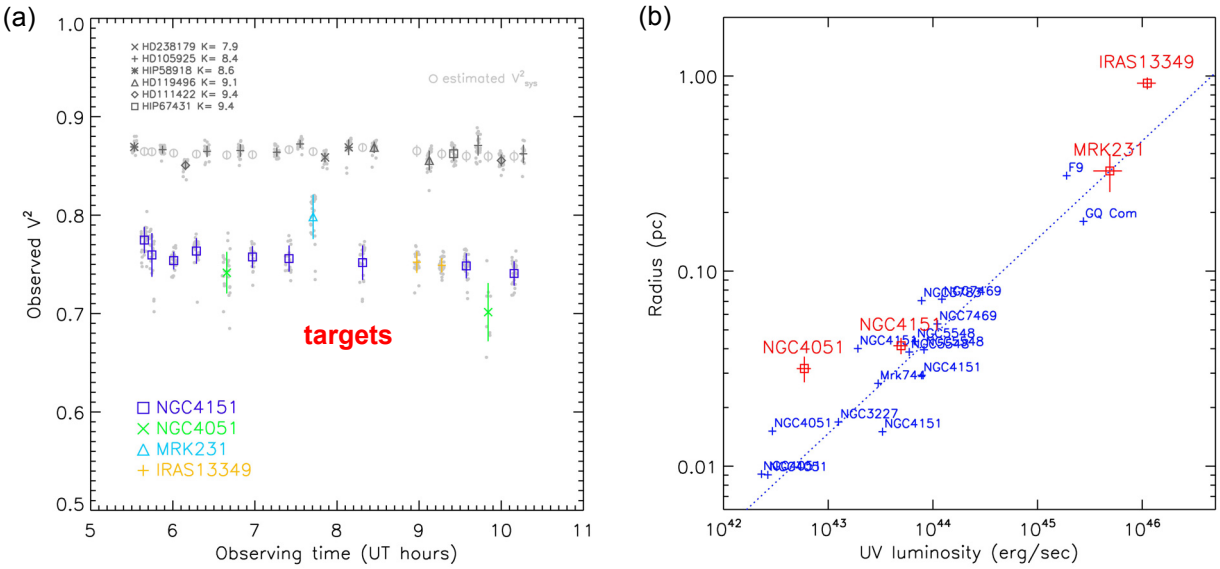

Figure 1: *(a) Observed squared visibilities V^2 for 4 AGNs and calibrators plotted against observing time. Gray dots are individual measurements for blocks of 5 s each. Light-gray circles are the estimated system V^2 (i.e. transfer function). Clear separations between calibrators and AGNs robustly show that these AGNs are spatially resolved. (b) Ring radius derived for each target (red squares), plotted against UV luminosity. Also shown in blue signs are the reverberation radii (Suganuma et al. 2006) and their fitted line (dotted line).*

The Characteristic Blue Spectra of Accretion Disks in Quasars as Uncovered in the Infrared

Quasars are thought to be powered by supermassive black holes accreting surrounding gas. Central to this picture is a putative accretion disk which is believed to be the source of the majority of the radiative output. It is well known, however, that the most extensively studied disk model (Shakura & Sunyaev 1973) — an optically thick disk which is heated locally by the dissipation of gravitational binding energy — is apparently contradicted by observations in a few major respects. In particular, the model predicts a specific blue spectral shape, $F_\nu \propto \nu^{+1/3}$, from the *visible* to the *near-infrared*, but the spectral shape at *visible* wavelengths is much redder than this prediction (e.g., Neugebauer et al. 1987).

A crucial observational difficulty was that toward the infrared, the disk spectrum starts to be hidden under strong, hot dust emission from much larger but hitherto unresolved scales, and thus has essentially been impossible to observe. However, we have now obtained observations of polarized light interior to the dust-emitting region that enable us to uncover this near-infrared accretion disk spectrum in several quasars. The revealed spectra show that the *near-infrared* disk spectrum is indeed as blue as predicted by the model above (*i.e.,* $F_\nu \propto \nu^{+1/3}$). This indicates that, at least for the outer near-infrared-emitting radii, the standard picture of the locally heated disk is approximately correct.

→ Kishimoto et al. 2008; PR 2008

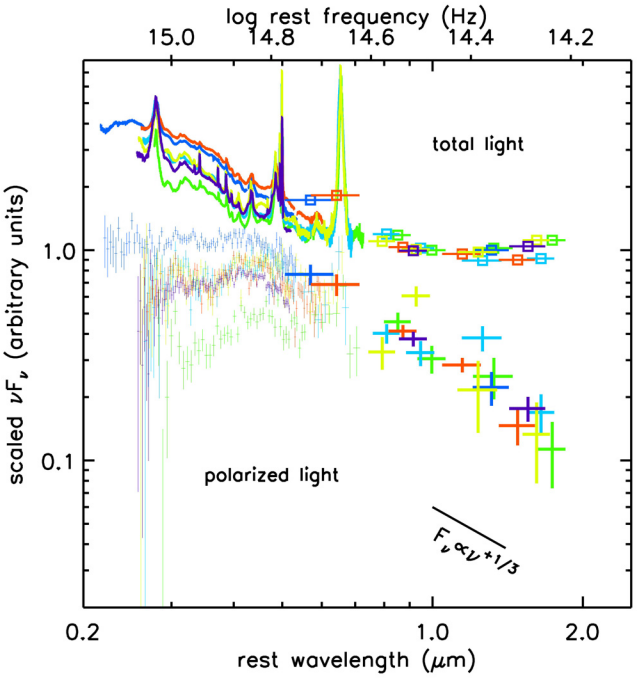

Figure 2: *Overlay of the polarized- and total-light spectra observed in six different quasars. We plot scaled νF_ν data: Q0144-3938 (redshift z = 0.244), green; 3C95 (z = 0.616), blue; CTS A09.36 (z = 0.310), light blue; 4C 09.72 (z = 0.433), red; PKS 2310-322 (z = 0.337), light green. Plotted in dark blue are the data for Ton 202 (z = 0.366) from Kishimoto et al. (2005). Total-light spectra, shown as bold lines in the optical and as squares in the near-infrared, are normalized at 1 μm in the rest frame. Polarized-light spectra, shown as light tiny dots with error bars in the optical (between 0.2 and 0.7 μm) and as bold plus signs in the near-infrared (with error bars), are also separately normalized at 1 μm. For clarity, the normalized polarized-light spectra are arbitrarily shifted downwards by a factor of three relative to the normalized total-light spectra. The total-light spectra in νF_ν turn up at around or slightly longward of 1 μm. In contrast, the polarized-light spectra in νF_ν all consistently and systematically decrease towards long wavelengths, showing a blue shape of approximately power-law form, consistent with $F_\nu \propto \nu^{+1/3}$.*

Parse-Scale Dust Distributions in Seyfert Galaxies: Results of the MIDI AGN Snapshot Survey

Active galactic nuclei are powered by the accretion of matter onto supermassive black holes in the centers of galaxies. A toroidal distribution of warm gas and dust is a key component in our current picture of AGNs. This so-called dusty torus is the reservoir of material for feeding the supermassive black hole, and it is the obscuring material which is made responsible for different manifestations of AGNs (type 1 and type 2 AGNs).

Only interferometric observations provide the angular resolution necessary to resolve the nuclear dust and to directly study its distribution and properties. In our MIDI AGN Snapshot Survey, a total of 10 AGNs were observed with MIDI at the VLTI. The goal was to determine the sizes of their dust distributions. Although the sources of the snapshot survey are close to the sensitivity limit of what can be observed with MIDI, for 7 of the 10 observed targets, scientifically useful data were obtained. The size estimates or limits derived from the interferometric data indicate that the dust distributions are compact, with sizes on the order of a few parsecs only.

Adding three sources with size estimates from previous MIDI measurements to the objects of the MIDI AGN Snapshot Survey, we found that the sizes s (Gaussian FWHM) of the nuclear dust distributions roughly scale as $s = p\, L_{MIR}^{0.5}$, where $p = 2 \cdot 10^{-18}$ pc $W^{-0.5}$ and L_{MIR} is the luminosity in the mid-infrared (see Fig. 3). This is in agreement with a model of nearly optically thick dust structures heated to $T \sim 300$ K. Except for the 10 µm silicate feature, there is no strong evidence for any difference in the dust distributions of type 1 and type 2 objects. It seems that the differences between individual galactic nuclei are greater than the generic differences between type 1 and type 2 objects in the mid-infrared (see also next section). → Tristram et al. 2009

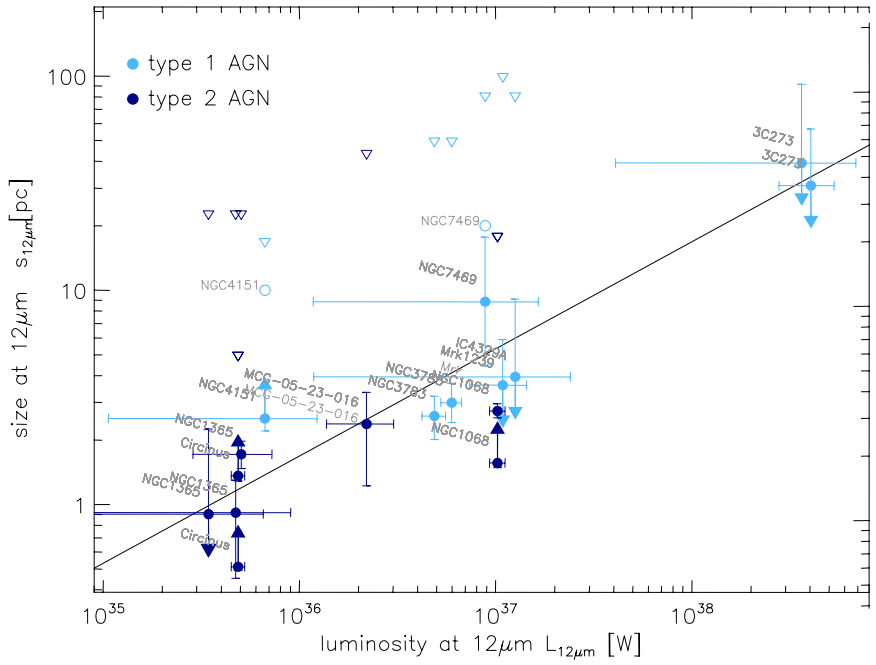

Figure 3: *Sizes (Gaussian FWHM) of AGN tori in the mid-infrared as a function of their monochromatic luminosities in the mid-infrared for the AGNs studied with MIDI (filled circles with error bars). Upper and lower limits on the size estimates are marked by arrows. The fitted size-luminosity relation for* $p = 1.8 \cdot 10^{-18}$ *pc* $W^{-0.5}$ *is traced by the black line. The size of the resolved emission in NGC 4151 (10 pc) from Neugebauer et al. (1990) and in NGC 7469 (~20 pc) from Soifer et al. (2003) are shown by open circles.*

Resolving the Obscuring Torus in NGC 1068 with the Power of Infrared Interferometry: Revealing the Inner Funnel of Dust

For a few nearby AGNs, more extensive studies of their nuclear dust distributions have been carried out with MIDI. One of the prime candidates for such a study is the well-known nucleus of NGC 1068, which is considered to be the prototype Seyfert 2 galaxy. Initial MIDI observations of NGC 1068

revealed warm (320 K) silicate dust in a 2.1×3.4 pc structure, surrounding a small hot (800 K) component whose shape and orientation could not be determined in detail (Jaffe et al. 2004).
New observations with MIDI at the VLTI led to a significantly improved uv coverage with a total of 16 uv points. We find the new measurements are consistent with emission from a compact 0.45×1.35 pc component (Gaussian FWHM) that is composed of hot (~800 K) silicate dust (brown structure in Fig. 4). We identify this component with the inner hot funnel region. This hot component has an absorption profile different from standard interstellar dust, and it shows evidence for clumpiness. The emission is co-linear, and likely co-spatial, with an H_2O megamaser disk, and therefore tilted by 45° with respect to the radio jet (cf. Fig. 4). A second more extended (3×4 pc) component of warm (~300 K) dust surrounds the inner hot dust. We identify this second component as the 'body' of the torus. It is mostly over-resolved by our interferometric measurements, and its properties are not well constrained.
Although in general agreement with the unified picture, the nucleus of NGC 1068 is irregular in several aspects: the orientation of the dust is tilted with respect to the jet, the position angle of the visible ionization cone does not match the position angle of the inner dust funnel, and the 9.7 µm silicate feature appears to be different from what is expected from the dust observed in the Milky Way. It is interesting to compare the NGC 1068 results with our previous observations of the Circinus galaxy, which is also a Seyfert 2 galaxy (Tristram et al. 2007). In Circinus, the dust distribution can also be represented by two components, as in NGC 1068. However, the innermost dust in the Circinus nucleus is at much lower temperatures than the 800 K dust seen in NGC 1068. Because of the jet-torus misalignment in NGC 1068 and the lack of hot dust in the inner torus of the Circinus galaxy, these two galaxies do not fully correspond to the simple picture of an edge-on doughnut suggested by the simplest unified schemes after all − nature appears to be more complicated. → Raban et al. 2009

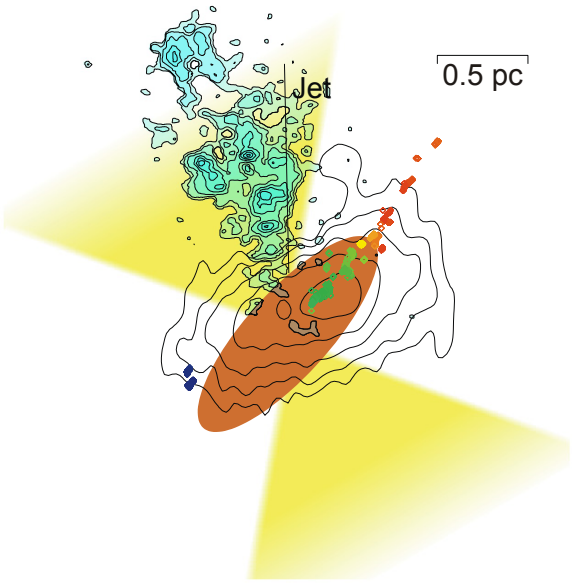

Figure 4: *Picture summarizing the multi-wavelength structures on parsec scales in the nucleus of NGC 1068. The FWHM of the compact (0.45×1.35 pc) and hot (~800 K) dust component is sketched in brown, centered around the H_2O maser spots and 5 GHz radio emission (from Gallimore et al. 2004; contour levels below the FWHM level have been removed to allow a better comparison between the radio and the mid-infrared). The ionization cones inferred from spectroscopy by Das et al. (2006) are shown in yellow, and the HST [O III] image (blue; reduced in scale by a factor of ~100; from Evans et al. 1991) is shown to indicate the orientation of the cone.*

Dust Emission from a Parsec-Scale Structure in the Seyfert 1 Nucleus of NGC 4151

A second very prominent object studied with MIDI in more detail is the Seyfert 1 galaxy NGC 4151. For this galaxy, observations with only two baselines have been obtained so far. For NGC 4151, observations are difficult for the VLTI since the target is located at DEC = +39. The resulting single-dish spectrum (solid line) with an effective aperture of ~300 mas is shown in the left panel of Figure 5 together with a Spitzer IRS spectrum (dashed line). The higher Spitzer flux most likely includes significant amounts of emission from the narrow-line region. The color temperature of the spectrum measured by MIDI is T = 285 ± 50 K. The two correlated flux spectra (baseline lengths of 61 and 89 m) are shown in the right panel of Figure 5. They are significantly below the values of the single dish spectrum, indicating that the warm thermal emission at the center of NGC 4151 is well resolved by the interferometer.

By comparing the data to a Gaussian model, we determined the diameter of the dust emission region, albeit only along one position angle, to be 2.0 ± 0.4 pc (FWHM) and to have an emissivity of ~0.1. These parameters are comparable to those in Seyfert 2 galaxies (see the two previous reports and Fig. 5). Using simple analytic temperature distributions, we find that the mid-infrared emission is probably not the smooth continuation of the hot nuclear source that is marginally resolved with K-band interferometry. We also detected weak excess emission around 10.5 µm, possibly indicating that silicate emission is extended to the parsec scale.
Due to the limited number of measurements, no two-dimensional information could be obtained, and questions about the unified model remain unanswered. Since nuclear dust distributions are different even within the same class of AGNs, the ultimate question whether or not the unified model is fully valid will not be answered before a statistical study of numerous tori is performed. Such a study is the goal of a new Large Program to observe several type 1 and type 2 AGNs with MIDI, which is currently being carried out. → Burtscher et al. 2009

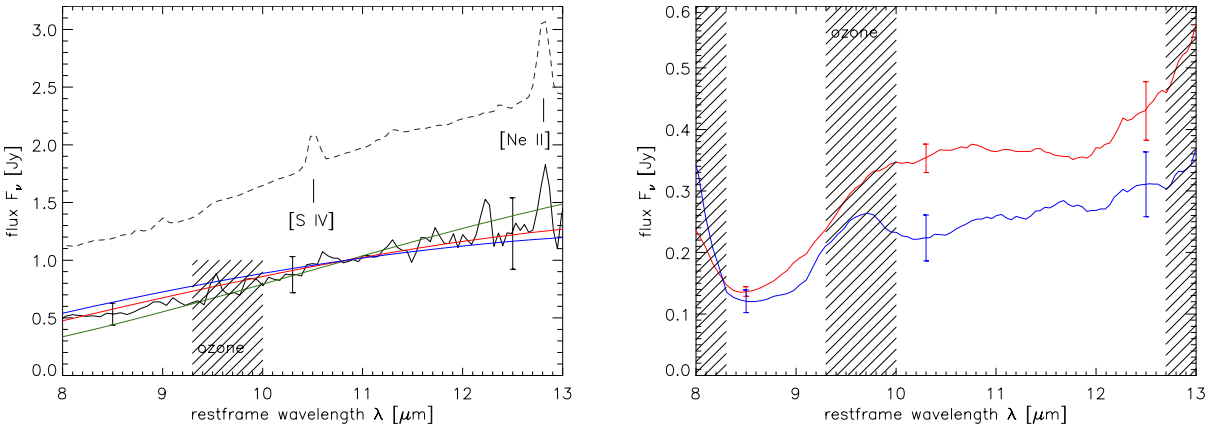

Figure 5: *Left: Single-dish spectra of NGC 4151: Spitzer spectrum (3.5 arcsec aperture, dashed; Weedman et al. 2005) and MIDI spectrum (0.3 arcsec aperture, black line with error bars). Also plotted are blackbody emission curves at T = 235, 285, 310 K (green, red, blue, respectively). Right: Smoothed (Δλ ~ 0.3 µm) correlated flux spectra at two different east–west projected baselines: 61 m (red) and 89 m (blue). The region of atmospheric ozone absorption, between 9.3 and 10.0 µm (hatched), is uncertain and not taken into account for the data analysis, as are the regions λ < 8.3 µm and λ > 12.7 µm (hatched), which have very low signal-to-noise ratios.*

The Radial Structure of AGN Tori derived from Infrared Interferometry

Over the last few years, it became possible to observe AGN tori with long-baseline interferometry both in the mid-IR and near-IR. However, most targets were only observed at one or two different baseline lengths. Since these AGNs reside at different distances and also have different physical torus sizes, an interferometric observation with a given baseline length probes a different spatial scale for each target. Therefore, it is apparently not straightforward to directly compare observations of different targets. We used the following technique to overcome this problem. We simply normalize the probed angular scale for each interferometric configuration by the angular size of the innermost radius of the torus R_{in} for each object. The size of R_{in}, as measured from optical-infrared reverberations, is known to scale with the AGN luminosity L as proportional to $L^{1/2}$ (Suganuma et al. 2006). Therefore, the normalization by R_{in} removes at least the simple $L^{1/2}$ luminosity dependence.
The normalization in angular sizes also removes the distance dependence. In this way, we can directly compare various data from various objects, uniformly view the data, and study whether or not the shapes of the intensity profiles of different AGN tori are similar.
Fig. 6 shows such a uniform look over available data. The spatial scale probed is shown in spatial frequency per R_{in} or its reciprocal "spatial wavelength" in units of R_{in} (see upper axis). We have color-coded the data so that information at different wavelengths can be directly compared. Here, we focused only on Type 1 AGNs (except for NGC 1068), since Type 1s are face-on-view objects and can thus be studied without significant inclination effects or position-angle dependence of the

baselines projected on the sky. Comparing the data with model visibilities, we estimated that the radial surface density distribution of directly illuminated material is roughly proportional to $r^0 - r^{-1}$, where r is the radius. → Kishimoto et al. 2009b

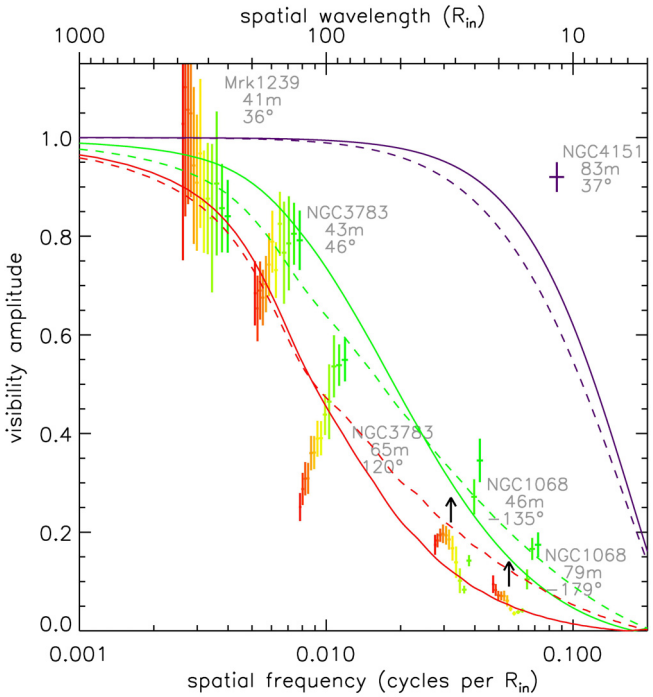

Figure 6: *Observed visibilities compared to a simple temperature gradient model. Red, green, and blue colors correspond to the observing wavelengths of 13, 8.5, and 2.2 μm, respectively. All AGNs (Mrk 1239, NGC 3783, NGC 4151) are Type 1 AGNs, except NGC 1068. Type 1s can be studied with less inclination effects. The data for NGC1068 are treated here as a lower limit. The object is thought to be inclined with the inner region obscured, making the observed brightness distribution more extended. This leads to a lower visibility, thus a lower limit for Type 1 cases. Solid curves correspond to a model surface density distribution proportional to $r^{0.0}$ for the large dust grain case, while dashed curves correspond to $r^{-0.9}$ for the standard ISM dust case.*

From Clumpy Torus Models to Physical Properties of Dust around AGN

In light of the great success of infrared interferometry within the last few years, we intensified our modeling efforts in order to be able to interpret observations of AGNs. For that, we improved our 3-D clumpy torus model (Hönig et al. 2006). In the past, we have already shown that the model is a hands-on tool to simultaneously model single-telescope infrared photometry and interferometry, for example, as applied to NGC 1068. Now, the improved models have been presented as tools to translate classical and interferometric observations into characteristic parameters of the dust distribution. We compared model SEDs for different chemical and grain-size compositions of the dust and found that clouds with standard ISM dust and optical depth $\tau_V \sim 50$ appear in overall agreement with observed IR SEDs. One of the main properties of the dust distribution in the torus is the radial cloud density distribution power law $\eta_r \propto r^a$ (corresponding to the number of clouds per unit length). By studying the parameter dependencies, it is shown that type 1 AGN SEDs can be used to constrain the radial dust cloud distribution power-law index a, as well as the mean number of clouds along an equatorial line of sight, N_0, which characterizes the obscuration in the torus. Possible parameter degeneracies with the vertical structure of the torus can be overcome by using interferometric data – either modeling the baseline-dependence or the wavelength-dependence of the visibility. Although type 2 AGNs can principally also be used to constrain model parameters, obscuration effects make the analysis more ambiguous. → Hönig & Kishimoto 2009, submitted; arXiv:0909.4539v1

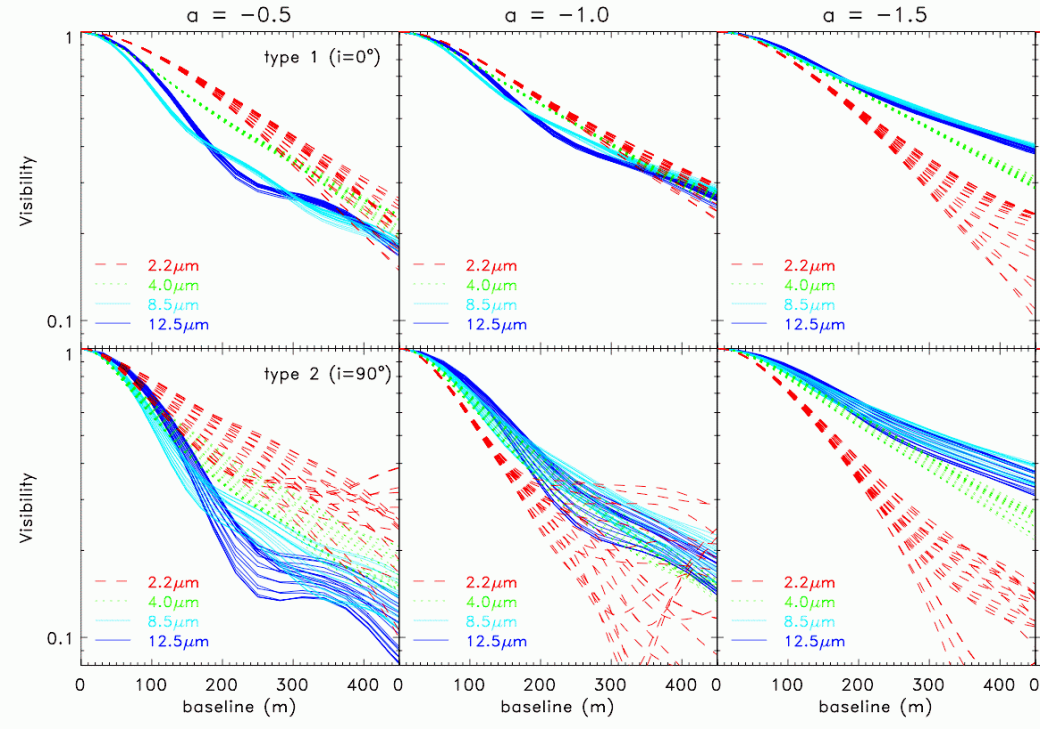

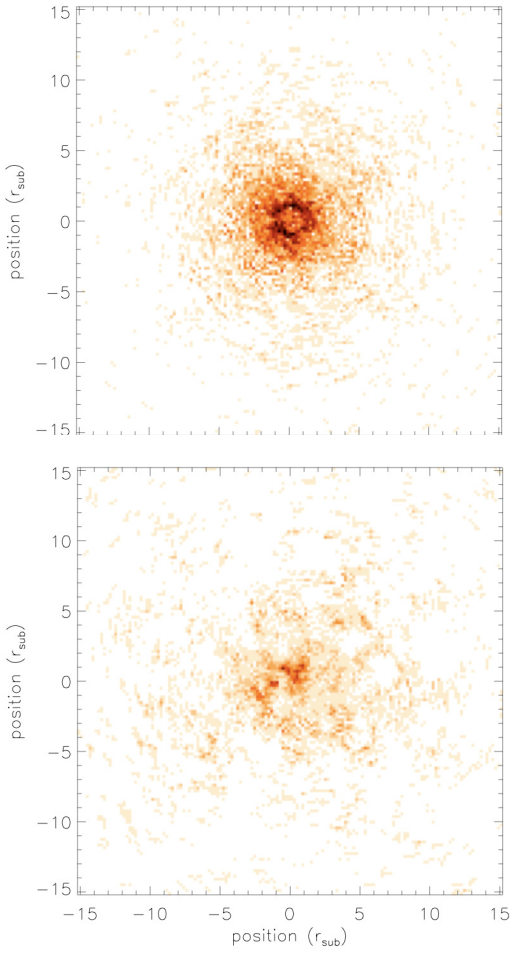

Figure 7: *Clumpy torus model radiative transfer images and infrared visibility study. Top: Dependence of the model visibility on the baseline for an AGN at 15 Mpc distance and a dust sublimation radius of 0.025 pc. Each column represents simulation results for a different radial dust cloud density distribution power law index $a = -0.5, -1.0, -1.5$, and -2.0, respectively, (top: type 1 AGN at $i = 0°$; bottom: type 2 AGN at $i = 90°$) with constant $N_0 = 5$. In each panel, we show visibility curves at 2.2 (red-dashed lines), 4.0 (green-dotted lines), 8.5 (light-blue solid lines), and 12.5 μm (dark-blue solid lines). The different lines per wavelength reflect the position-angle dependence of the visibility and can also be taken as a proxy for the variance that can be expected for different random arrangements of clouds in 3-D space for the same set of model parameters. Bottom: Model images (FOV 30×30 sublimation radii) at 8 μm for a face-on type 1 torus (top) and an edge-on type 2 torus (bottom).*

Discovery of a Strong Baldwin Effect in Mid-Infrared AGN Lines

The Baldwin effect, a negative correlation between the equivalent width W_λ of an emission line and the ionizing continuum luminosity L, is commonly found in broad and narrow UV/optical emission lines of AGNs, as well as in the iron Kα line in the X-rays. Although this effect has been known for about 3 decades, its physical origin remains a mystery. It is probably related to a change of shape of the AGN continuum emission with luminosity, which is responsible for ionizing the atoms.
Within the past years, we have collected ground-based mid-infrared spectro-photometry of a number of nearby AGNs with spatial resolution < 100 pc. The observations were carried out using the VLT/VISIR imager and spectrograph at the ESO/Paranal observatory. These 8−13 μm spectra show both dust continuum emission and some narrow forbidden atomic emission lines. In our initial sample of 8 objects, we discovered a Baldwin effect for the three most prominent emission lines [ArIII](8.99 μm), [SIV](10.51 μm), and [NeII](12.81 μm). From a comparison of the ionization potential of our mid-infrared lines (30−40 eV) to optical narrow emission lines, we would have expected a quite weak Baldwin effect. We found, however, an anticorrelation of approximately $W_\lambda \propto L^{-0.7}$ for these lines (for details, see Fig. 8), in contrast to power-law indices of -0.1 to -0.2 for UV/optical lines. Moreover, the bulk of the mid-infrared line emission originates in the inner ~0.4 arcseconds of the narrow-line region, unlike the prominent, extended fan-like emission seen in optical lines. This came as a complete surprise and might indicate that the underlying mechanism causing the Baldwin effect in the mid-infrared is different from the optical. We speculate that there might be gas-density variations in the innermost part of the narrow-line region which influence the forbidden line emission. → Hönig et al. 2008

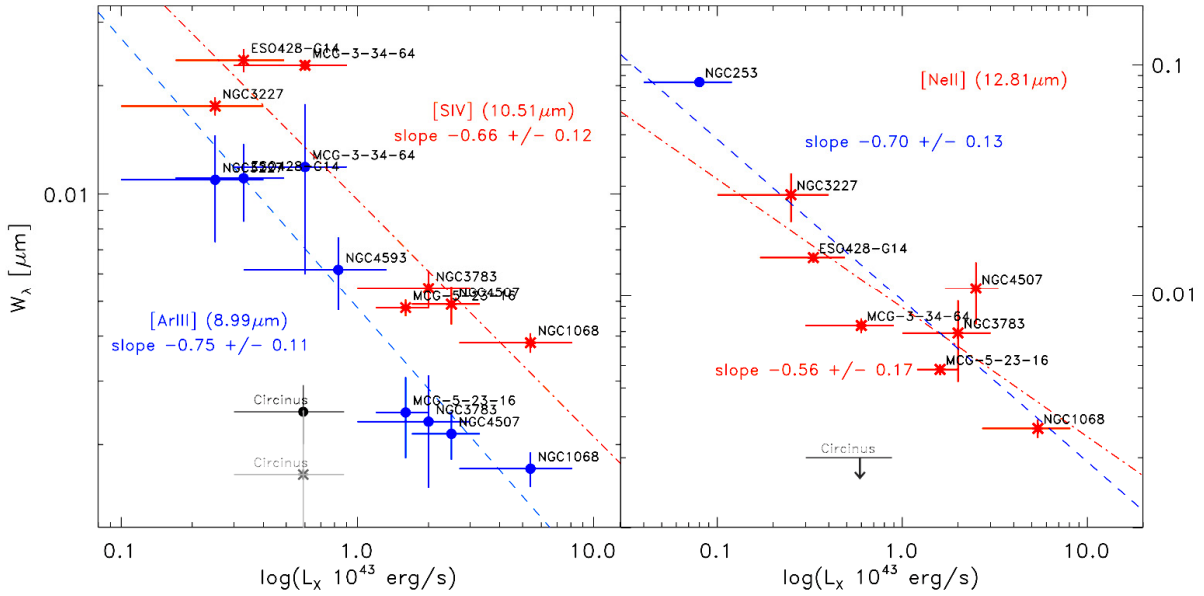

Figure 8: *The Baldwin effect in mid-infrared lines. Left: Equivalent width W_λ of the [ArIII] (blue circles) and [SIV] (red crosses) lines plotted against the X-ray luminosity LX for our sample of 8 nearby AGN. The fitted correlations $W_\lambda \propto L^{-0.75\pm0.11}$ for [ArIII] (blue dashed line; $\rho_{Spearman} = -0.91$, null-hypothesis probability 2×10^{-3}), and $W_\lambda \propto L^{-0.66\pm0.12}$ for [SIV] (red dashed-dotted line; $\rho_{Spearman} = -0.79$, null-hypothesis probability 4×10^{-2}) are shown. Circinus (gray symbols) is an outlier, probably because of significant dust obscuration in the host galaxy or the circumnuclear dust torus. Right: Equivalent width W_λ of the [NeII] line (red crosses) plotted versus the X-ray luminosity L_X (used as ionizing luminosity tracer) for 7 nearby Seyfert galaxies. The fitted correlation $W_\lambda \propto L^{-0.56\pm0.17}$ ($\rho_{Spearman} = -0.75$, null-hypothesis probability 5×10^{-2}) is shown as a red, dash-dotted line. When including NGC 253 (blue circle) − despite its questionable AGN nature – a correlation $W_\lambda \propto L^{-0.70\pm0.13}$ ($\rho_{Spearman} = -0.83$, null-hypothesis probability 1×10^{-2}) is found (blue dashed line). An upper limit to the measurement for Circinus (gray arrow) is given. The non-detection of [NeII] from the nuclear point source is probably due to significant dust obscuration in either the host galaxy or circumnuclear dust torus.*

Revealing the Torus Structure of Nearby AGN by High-Spatial Resolution Mid-IR Spectro-Photometry of Seyfert Galaxies and Clumpy Torus Modeling

We acquired mid-IR imaging and 8−13 μm low-resolution spectroscopy of nine type 1 and ten type 2 AGNs. The observations were carried out using the VLT/VISIR mid-IR imager and spectrograph and can be considered the largest currently available mid-infrared spectro-photometric data set of AGNs at spatial resolution < 100 pc. These data resolve scales at which the emission from the dust torus dominates the overall flux, and emission from the host galaxy (e.g., star formation) is resolved out in most cases. The silicate absorption features are moderately deep, and emission features, if seen at all, are shallow. We compared the observed mid-IR luminosities of our objects to AGN luminosity tracers (X-ray, optical, and [OIII] luminosities) and found that the mid-IR radiation is emitted quite isotropically. In two cases, IC 5063 and MCG–3–34–64, we find evidence for extended dust emission in the narrow-line region. We confirm the correlation between observed silicate feature strength and hydrogen column density, which was recently found in Spitzer data at lower spatial resolution. In a further step, our 3-D clumpy torus model was used to interpret the data. We show that the strength of the silicate feature and the mid-IR spectral index α (alpha) can be used to get reasonable constraints on the radial dust cloud distribution of the torus and the average number of clouds N_0 along an equatorial line-of-sight in clumpy torus models. The mid-IR spectral index α is almost exclusively determined by the radial dust cloud density distribution power-law index a (letter a), and the silicate feature depth mainly depends on N_0 and the torus inclination. A comparison of model predictions for our type 1 and type 2 AGNs reveals that average parameters of $a = -1.0 \pm 0.5$ and $N_0 = 5–8$ are typically seen in the presented sample, which means that the radial dust distribution is rather shallow. As a proof-of-concept of this method, we compared the model parameters (derived from α and the silicate feature strength) to more detailed studies of full IR SEDs and to existing interferometric data and found that the constraints on a and N_0 are consistent. Finally, we might have found evidence that the radial structure of the torus changes with AGN luminosity towards steeper dust distributions, and we discuss implications for the IR size-luminosity relation. → Hönig et al. 2009, submitted

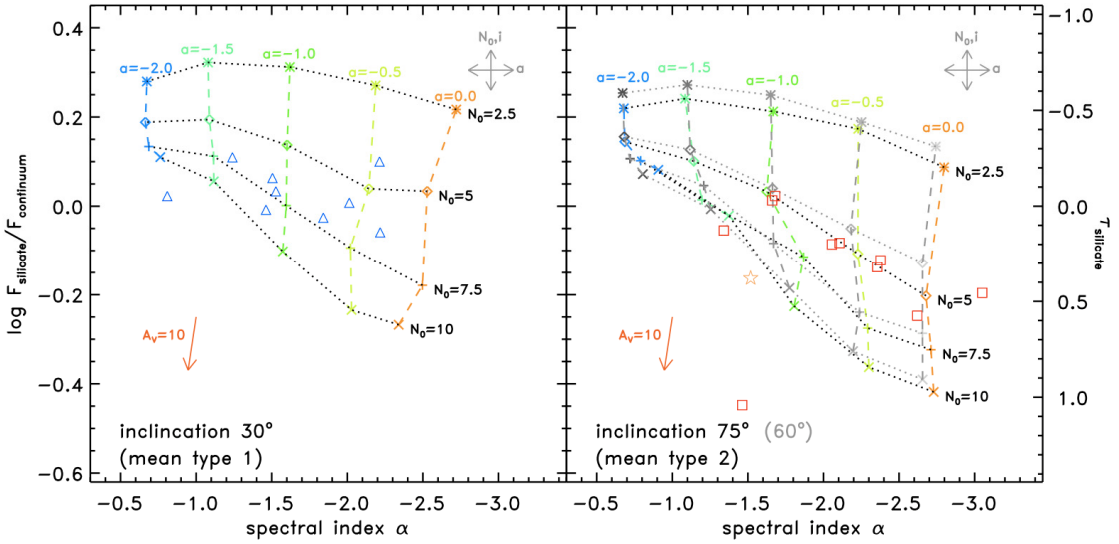

Figure 9: *Comparison of observed mid-IR properties of our type 1 and type 2 AGNs to model SEDs simulated with our 3-D clumpy torus model. Left: Silicate feature strength (and related optical depth) of the type 1 sub-sample (blue triangles) plotted against the spectral index α of the mid-IR continuum emission. Overplotted are model predictions for parameters ranging from cloud density distribution power law index a = 0.0 (orange) to a = -2.0 (light blue) and N_0 = 2.5 (asterisks) to N_0 = 10 (x-shapes) for a mean type 1 inclination of i = 30°. The gray arrows note the directions in which the model points change when varying a, N_0, and i. Right: Silicate feature strength (and related optical depth) of the type 2 sub-sample (red squares) plotted against the spectral index α of the mid-IR continuum emission. Overplotted are model predictions for the same parameter ranges as in the left panel for a mean type 1 inclination of i = 75° (colored symbols) and i = 60° (gray symbols, illustrating the inclination effect). The gray arrows are a rough illustration as a guide for the reader in which direction the model points mostly change when varying a, N_0, and i. For reference, NGC 1068 is shown as an orange star.*

Observing the Mid-Infrared Cores of Local Seyfert Galaxies and Strengthening the Mid-Infrared/X-Ray Luminosity Correlation

We present new photometry of 16 local Seyferts, including 6 Compton-thick sources in N-band filters around 12 μm. The data were obtained using the VISIR instrument at the VLT observatory. Since most of the sources are too weak for interferometry, this near-diffraction-limited imaging provides the least-contaminated core fluxes for these sources to date. Augmenting these with our previous observations and with published intrinsic X-ray fluxes, we form a total sample of 42 sources, for which we find a strong mid-infrared/X-ray (12.3 μm/2-10 keV) luminosity correlation. Now, this correlation is well established for spatial scales < 100 pc and both type 1 and type 2 AGNs. Performing a sub-selection of sources in which the Seyfert torus is likely to be "well isolated" (= intrinsic spatial resolution < 500 sublimation radii) results in the correlation $L_{MIR} \propto L_X^{1.11\pm0.07}$, with a reduction of the scatter in luminosities as compared to the full sample. This is much tighter than any such correlation found before for lower spatial resolution in the mid-infrared. One of the most surprising results is that unobscured, obscured, and Compton-thick sources all closely follow the same luminosity correlation within a factor of < 2−3. This may have important implications for the structures of Seyfert cores since it suggests that the mid-infrared luminosity is emitted quite isotropically. The typical resolution limit of our imaging corresponds to ~70 pc at a median of $z = 0.01$, and we use the tightness of the correlation to place constraints on the dominance of any residual emission source within these physical scales. An upper limit for any contaminating star formation of ~40% of the unresolved flux is inferred, on average. → Gandhi et al. 2009

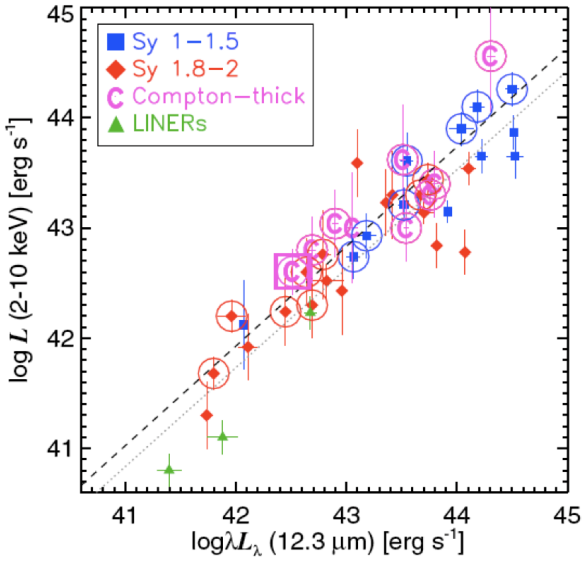

Figure 10: *Mid-infrared/X-ray luminosity correlation for the sample of 43 VISIR detections. In the plot, we distinguish between type 1 AGNs (blue squares), Compton-thin type 2 AGNs (red diamonds), Compton-thick type 2 AGNs (light-red C; X-ray luminosity derived from 20−100 keV data), and LINERs (green triangles). The sources classified as being "well-isolated" are circled, and the diagonal dashed line is the fitted correlation for these. The dotted grey line is the correlation fit to all 43 sources.*

YOUNG STELLAR OBJECTS

Revealing the Sub-AU Asymmetries of the Inner Dust Rim in the Disk Around the Herbig Ae Star R CrA

Unveiling the structure of the disks around intermediate-mass pre-main-sequence stars (Herbig Ae/Be stars) is essential for our understanding of the star- and planet-formation process. In particular, models predict that in the innermost AU around the star, the dust disk forms a "puffed-up" inner rim, which should result in a strongly asymmetric brightness distribution for disks seen under intermediate inclination.

Using the VLTI/AMBER long-baseline interferometer, we obtained 24 near-infrared (H- and K-band) spectro-interferometric observations of R CrA, which is a Herbig Ae star in the nearby (d = 130 pc) Corona Australis molecular cloud. Observing with three telescopes in a linear array configuration, each data set samples three equally spaced points in the visibility function, providing direct information about the radial intensity profile. In addition, the observations cover a wide position angle range (~97°), probing the position angle dependence of the source brightness distribution.

In the derived visibility function, we detect the signatures of an extended (Gaussian FWHM ~ 25 mas) and a compact component (Gaussian FWHM ~ 5.8 mas), with the compact component contributing about two-thirds of the total flux. The brightness distribution is highly asymmetric, as indicated by the strong closure phases (up to ~40°). To interpret these asymmetries, we employed various geometric as well as physical models, including a binary model, a skewed ring model, and a puffed-up inner rim model with a vertical or curved rim shape. For the binary and vertical rim models, no acceptable fits could be obtained. On the other hand, the skewed ring model and the curved puffed-up inner rim model allow us to simultaneously reproduce the measured visibilities and closure phases. From these models we derive the location of the dust sublimation radius (~0.4 AU), the disk inclination angle (~35°), and a north-south disk orientation (PA ~ 180−190°).

Our curved, puffed-up rim model (Fig. 11a-b) can simultaneously reproduce the SED (Fig. 11c) and the interferometric observables (Fig. 11d−e) reasonably well and suggests a luminosity of ~29 $L_{\odot}$ and the presence of relatively large (~1.2 µm) silicate dust grains. Perpendicular to the disk, two bow-shock-like structures appear in the associated reflection nebula NGC 6729, suggesting that the detected sub-AU-size disk is the driving engine of a large-scale outflow. → Kraus et al. 2009

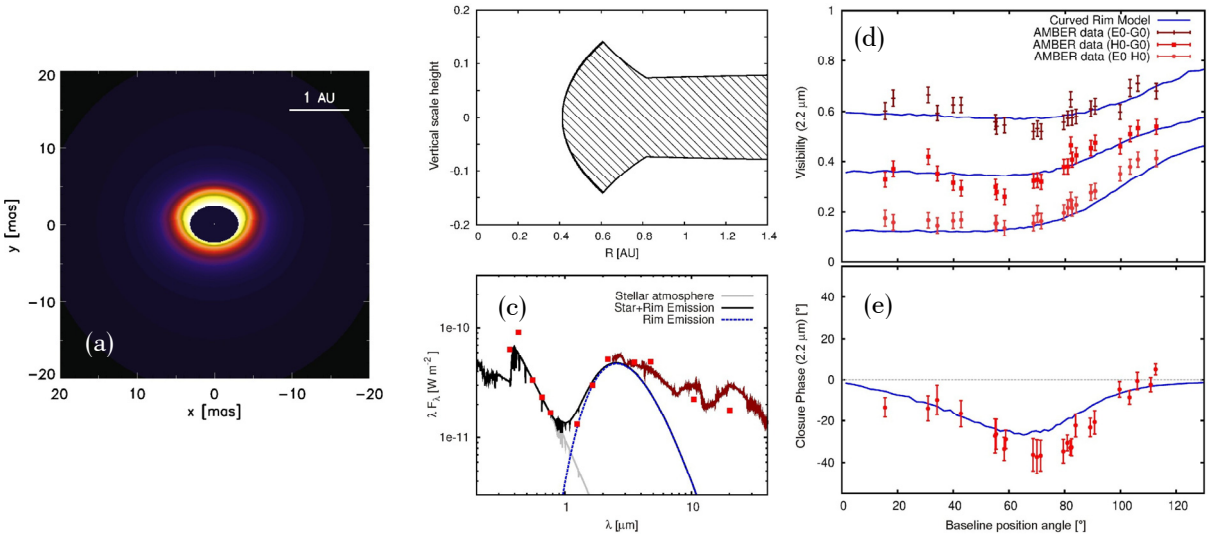

Figure 11: *Using a puffed-up dust rim model (a: model image; b: vertical disk scale height) allows us to simultaneously reproduce the near-infrared SED of R CrA (c), as well as the interferometric visibilities (d) and closure phases measured by VLTI/AMBER (e).*

The Origin of Hydrogen Line Emission for five Herbig Ae/Be Stars Spatially and Spectrally (λ/Δλ=1500) Resolved by VLTI/AMBER Spectro-Interferometry

Besides their characteristic infrared excess continuum emission, Herbig Ae/Be stars are known to show line emission, for instance from hydrogen. Although this has been known for decades, the spatial origin of the line emission is still strongly debated. For instance, it has been suggested that the Br γ line at 2.16 μm traces gas which is being accreted onto the star through magnetospheric accretion columns, while others associate the line emission with mass outflow processes (stellar winds, X-winds, or disk winds; Fig. 12, top).

Using the medium spectral resolution mode of the VLTI/AMBER instrument, we spatially and spectrally (λ/Δλ = 1500) resolved the AU-scale environment of five Herbig Ae/Be stars (HD 163296, HD 104237, HD 98922, MWC 297, V921 Sco) in the Br γ emission line as well as in the continuum. From the measured wavelength-dependent visibilities, we derive the size of the continuum and Br γ line-emitting region (Fig. 12, bottom). Additional information is provided by the measured closure phases. For all objects (except MWC 297), we measure an increase of visibility within the Br γ emission line, indicating that the Br γ-emitting region in these objects is more compact than the dust sublimation radius. For HD 98922, our quantitative analysis reveals that the line-emitting region is compact enough to be consistent with the magnetospheric accretion scenario. For HD 163296, HD 104237, MWC 297, and V921 Sco, we identify an extended stellar wind or a disk wind as the most likely line-emitting mechanism. Since the stars in our sample cover a wide range of stellar parameters, we also search for general trends and find that the size of the Br γ-emitting region does not seem to depend on the basic stellar parameters (such as the stellar luminosity), but correlates with spectroscopic properties, in particular with the Hα line profile shape.

By performing the first high-resolution spectro-interferometric survey on Herbig Ae/Be stars, we find evidence for at least two distinct Br γ line-formation mechanisms. Most significant, stars with a P-Cygni Hα line profile and a high mass-accretion rate seem to show particularly compact Br γ-emitting regions ($R_{\mathrm{Br}\,\gamma}/R_{\mathrm{cont}} < 0.2$), while stars with a double-peaked or single-peaked Hα-line profile show a significantly more extended Br γ-emitting region ($0.6 < R_{\mathrm{Br}\,\gamma}/R_{\mathrm{cont}} < 1.4$), possibly tracing a stellar wind or a disk wind. → Kraus et al. 2008

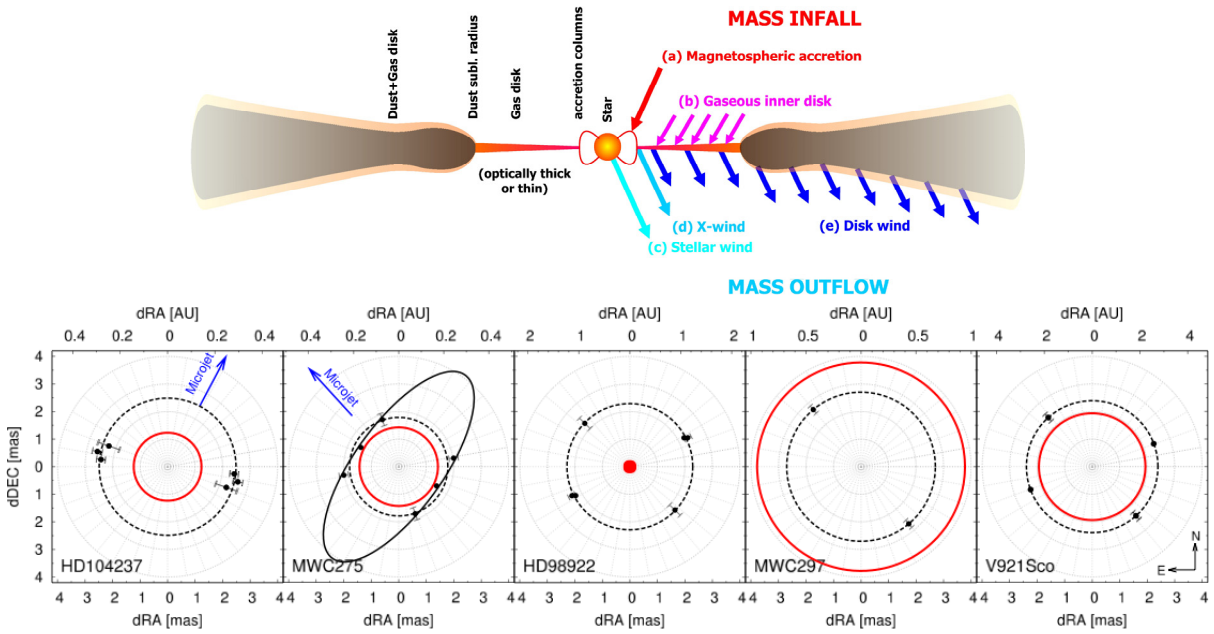

Figure 12: *Top: Various scenarios have been proposed for the origin of the line emission in YSOs, including mass infall processes and mass outflows. Bottom: Characteristic sizes, as derived from our VLTI/AMBER spectro-interferometry on five Herbig Ae/Be stars in the continuum (black circles/ellipses) and in the Br γ line (red circles). For four objects (HD 104237, MWC 275, MWC 297, V921 Sco), we measured a spatially extended Br γ-emitting region, suggesting that the line emission originates in a stellar or disk wind. Only one object (HD 98922) exhibits an unresolved line-emitting region, as expected for an origin in magnetospheric accretion.*

Strong Near-Infrared Emission in the Sub-AU Disk of the Herbig Ae Star HD 163296: Evidence of Refractory Dust?

Herbig Ae/Be stars are pre-main sequence stars of intermediate mass (~2−10 $M_{\odot}$). Investigating the properties of matter within the innermost AU is crucial for our understanding of star and planet formation. The first interferometric studies of Herbig Ae/Be stars showed that the near-infrared characteristic sizes were larger than expected by classical accretion disk models (Millan-Gabet et al. 2001) and were found to be correlated with the stellar luminosity (Monnier & Millan-Gabet 2002). This supports the idea that the near-infrared emission is dominated by the thermal emission of hot dust heated by stellar radiation. However, various recent observations have shown that this scenario is not sufficient to explain the AU-scale morphology of all Herbig Ae/Be stars. Instead, several objects require an additional hot and compact emission component (e.g. Eisner et al. 2007, Kraus et al. 2008, Tatulli et al. 2008, Tannirkulam et al. 2008).

In order to further investigate the physical nature of this compact (sub-AU) near-infrared emitting component, we investigated the Herbig Ae star HD 163296 (MWC 275) using the VLTI/AMBER instrument (Fig. 13). Our *H*- and *K*-band observations have a spectral resolution of ~30 and cover a range of spatial resolutions between ~3 and ~12 milli-arcseconds. Furthermore, our data set represents one of the most comprehensive uv coverages achieved for a young star so far. The circumstellar material is resolved at the sub-AU spatial scale, and closure phase measurements indicate a small but significant deviation from point symmetry. We discuss the results assuming that the near-infrared excess in HD 163296 is dominated by the emission of a circumstellar disk. A successful fit to the spectral energy distribution, near-infrared visibilities, and closure phases is found with a model in which a dominant contribution to the H- and K-band emission originates in an optically thin, smooth, and point-symmetric region extending from about 0.1 to 0.45 AU. At a distance of 0.45 AU from the star, silicates condense, and the disk becomes optically thick and develops a puffed-up rim, whose skewed emission can account for the non-zero closure phases. We discuss the source of the inner (<0.45 AU) disk emission and tentatively exclude dense molecular gas as well as optically thin atomic or ionized gas as its possible origin. Instead, we propose that the smooth inner emission is produced by very refractory grains in a partially cleared region. If so, we may be observing the disk of HD 163296 just before it reaches the transition disk phase. → Benisty et al., in press; arXiv: 0911.4363v2

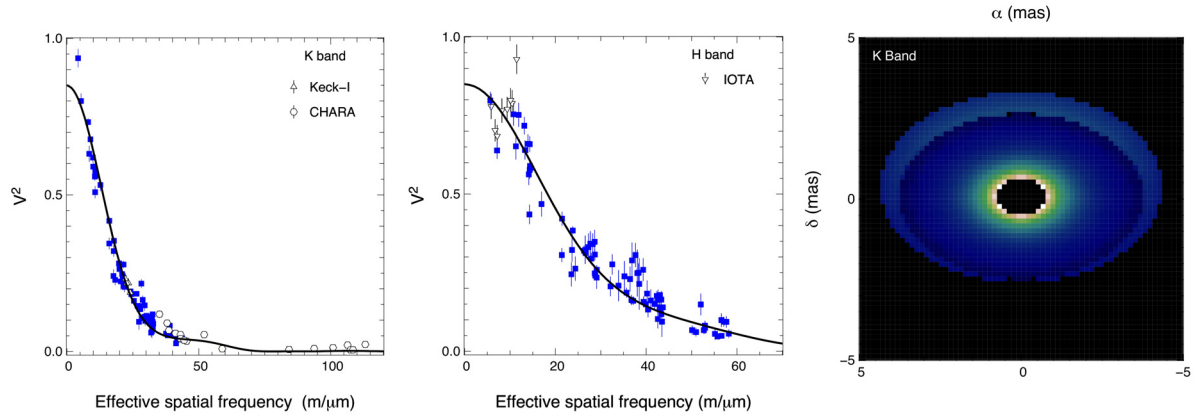

Figure 13: *For the Herbig Ae star HD 163296, we collected a large amount of K- (left) and H-band (middle) visibility measurements, including our new VLTI/AMBER measurements (blue square symbols) as well as literature measurements obtained with the Keck and IOTA interferometer (triangles) and the CHARA array (dots). We find that the data set can be reproduced assuming a dust disk with a puffed-up inner rim and an additional hot inner emission component, possibly composed of highly refractory dust grains, for instance of iron.*

VLTI/AMBER Aperture-Synthesis Imaging of θ1 Orionis C: Tracing the Young, Massive High-Eccentricity Binary System through Periastron Passage

The nearby high-mass star θ^1 Ori C (O5−O7) is the brightest and most massive of the Trapezium OB stars at the core of the Orion Nebula Cluster, and it represents a perfect laboratory to determine the fundamental parameters of young hot stars. Since the discovery of θ^1 Ori C's companion by our group, we have traced its orbital motion with the aim of determining the orbit and dynamical mass. In addition to a characterization of the individual components, ultimately, this will yield new constraints for stellar evolution models in the high-mass regime. In 2007/2008, we observed θ^1 Ori C with VLTI/AMBER long-baseline interferometry (NIR H and K bands), as well as with bispectrum speckle interferometry (B and V band). Combining AMBER data taken with three different 3-telescope configurations, we reconstructed the first VLTI/AMBER aperture-synthesis image of θ^1 Ori C (separation ~ 19 mas; Fig. 14 right). The derived orbital elements imply a short-period ($P \sim 11.3$ yr) and high-eccentricity ($e \sim 0.6$) orbit. The observations are consistent with recently published radial velocity measurements, from which we can derive direct constraints on the mass ratio ($M_1/M_2 = 0.22 \pm 0.05$). We derive the system mass ($M_{\rm system} = 44 \pm 7\ M_\odot$) and the dynamical distance ($d = 410 \pm 20$ pc), which is in good agreement with trigonometric parallax measurements obtained with radio interferometry ($d = 414 \pm 7$ pc; Menten et al. 2007). → Kraus et al. 2009 & PR 2009

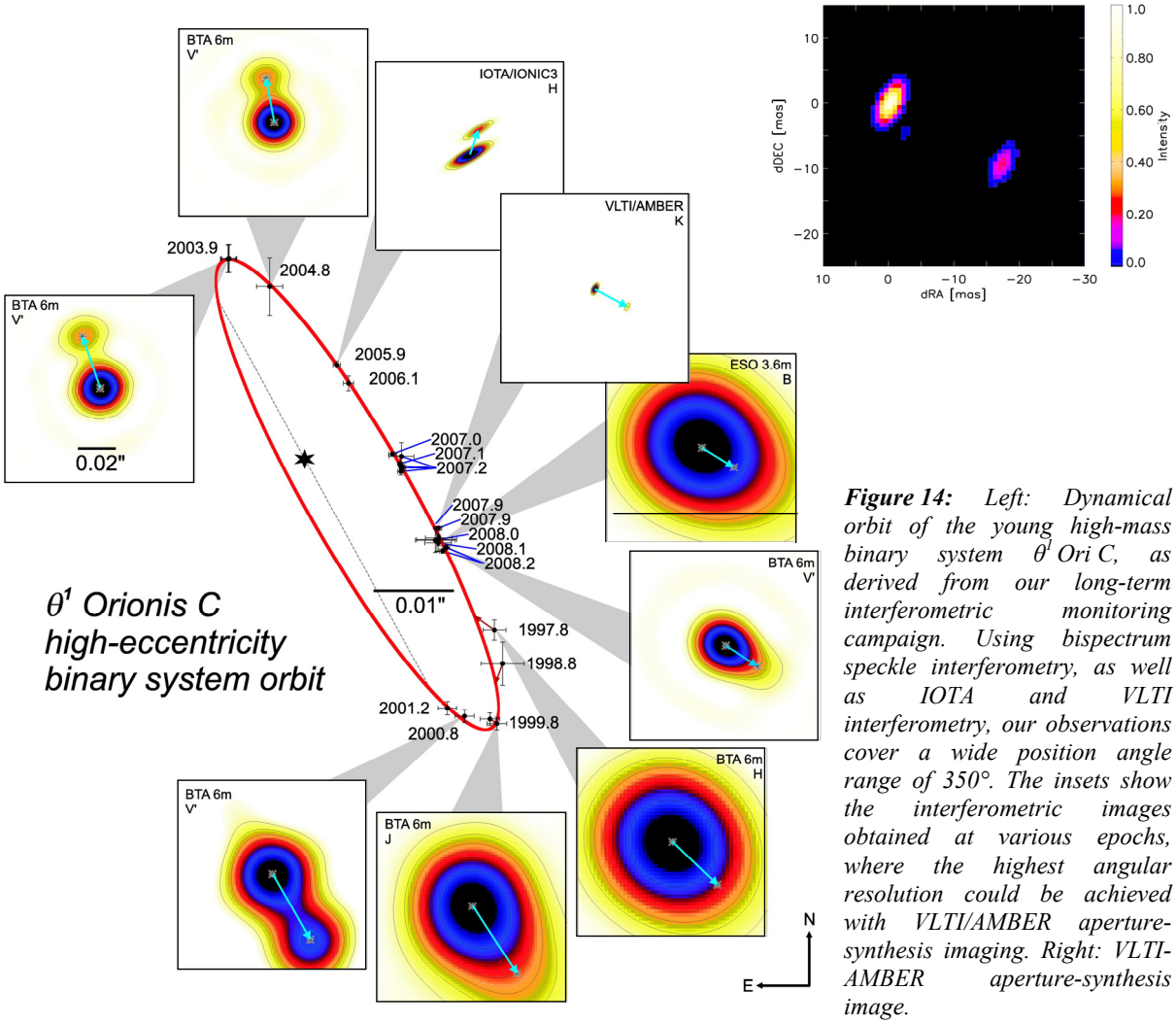

Figure 14: *Left: Dynamical orbit of the young high-mass binary system θ^1 Ori C, as derived from our long-term interferometric monitoring campaign. Using bispectrum speckle interferometry, as well as IOTA and VLTI interferometry, our observations cover a wide position angle range of 350°. The insets show the interferometric images obtained at various epochs, where the highest angular resolution could be achieved with VLTI/AMBER aperture-synthesis imaging. Right: VLTI-AMBER aperture-synthesis image.*

First VLTI Spectro-Interferometry of a YSO with a Spectral Resolution of 12000: The Gas Distribution around the Herbig Be Star MWC 297

Circumstellar disks play a fundamental role in the formation of stars and planets. The inner circumstellar region hosts fascinating astrophysical phenomena such as gaseous accretion disks, disk winds, jets, dust sublimation, etc. NIR interferometry with high spectral resolution is able to spatially resolve the gas and dust distribution in the inner AU- and sub-AU regions of disks and constrain their physical properties. Therefore, such observations allow us to probe the nature of the accretion process and the launching of jets and winds. For the more luminous Herbig Be stars, optically thick gaseous disks, which extend well inside the dust sublimation radius, seem to play an important role. Some of the observed emission lines are possibly emitted by matter which is being ejected from the system rather than from the gaseous accretion disk itself.

The Herbig Be star MWC 297 is one of the closest (~250 pc) young, massive (~10 $M_{\odot}$; B1.5V) stars. Our AMBER/VLTI/fringe tracker observations of MWC 297 in Fig. 15 are the first IR interferometric observations of a YSO with a high spectral resolution of 12000. This high spectral resolution is crucial for studying the visibilities and closure phases in several different spectral channels within a Doppler-broadened line (see Fig. 15a). We derived the size and asymmetry of both the continuum- and the line-emitting region in many spectral channels within the Brackett γ emission line. At the center of the Br γ line, we measured a Gaussian radius (HWHM) of 7 mas (1.7 AU; see Fig. 15b). In the continuum, we obtained a much smaller HWHM radius of 2.2 mas (~0.5 AU). This resolved compact 0.5 AU continuum structure is likely a dense gaseous accretion disk, since it is ~6 times smaller than the dust sublimation radius (~3 AU). The line-emitting region (likely the disk wind region) is ~3 times larger than the continuum-emitting disk region. To explain the wavelength dependence of the visibilities and phases, we performed detailed 3-D radiative transfer modeling

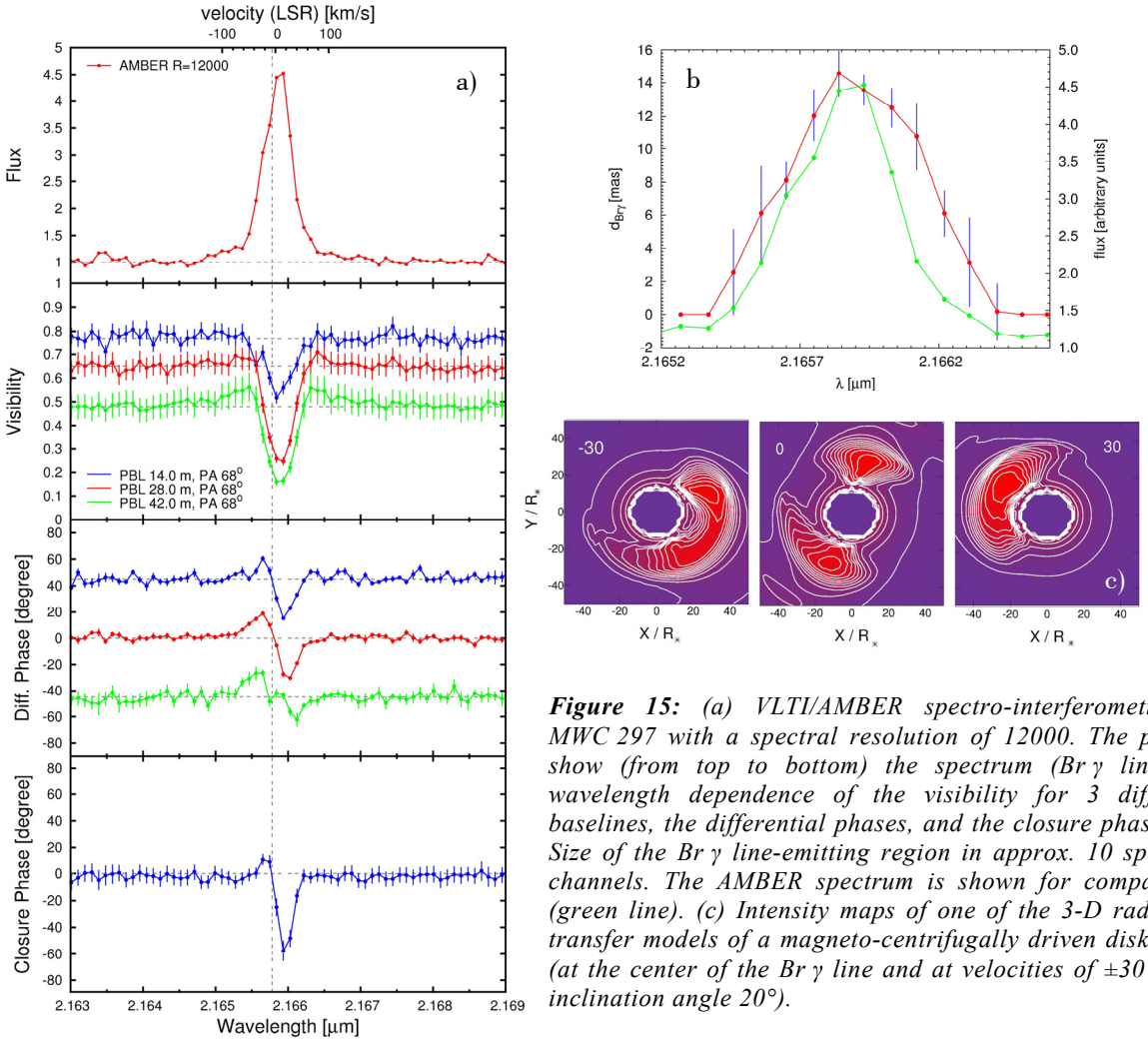

Figure 15: *(a) VLTI/AMBER spectro-interferometry of MWC 297 with a spectral resolution of 12000. The panels show (from top to bottom) the spectrum (Br γ line),the wavelength dependence of the visibility for 3 different baselines, the differential phases, and the closure phase. (b) Size of the Br γ line-emitting region in approx. 10 spectral channels. The AMBER spectrum is shown for comparison (green line). (c) Intensity maps of one of the 3-D radiative transfer models of a magneto-centrifugally driven disk-wind (at the center of the Br γ line and at velocities of ±30 km/s; inclination angle 20°).*

using a magneto-centrifugally driven disk-wind model (Blandford & Payne 1982, Grinin & Mitskevich 1990, Tambovtseva et al. 2001) of a gaseous accretion disk inside the dust sublimation radius. Figure 15c shows intensity maps of one of our models at the center of the Br γ line and at velocities of ±30 km/s. Our results show that the best fit is obtained for disk-wind models with large opening angles (up to 80°) and inclination angles from 10 to 30°.

Near-Infrared Imaging Polarimetry of the High-Mass Protostar CRL 2136, the Intermediate-Mass Herbig Be Star R Mon, and the Low-Mass Star HL Tau

Imaging polarimetry is a powerful technique to probe the dusty disks of YSOs because polarimetry efficiently detects scattered light. In many polarization images of bipolar reflection nebulae, so-called polarization disks are observed. Using the NACO/VLT and CIAO/Subaru AO instruments, we performed imaging polarimetry of the low-mass protostar HL Tau, the Herbig Be star R Mon (Fig. 16a), and the high-mass protostar CRL 2136 (Fig. 16b-c) to investigate their circumstellar dust distribution and grain properties. Combining imaging polarimetry with radiative transfer modeling allowed us to investigate the geometry and grain properties of CRL 2136's disk (Fig. 16b-c). CRL 2136 is a young high-mass (~20 $M_\odot$) star. Fig. 16c shows a polarization image of CRL 2136. The polarization disk with a polarization vector alignment approximately parallel to the polarization disk extends along the PA of ~45°, which is orthogonal to the outflow direction. In order to model the disk, we developed a Monte Carlo radiative transfer code (STSH code; Murakawa et al. 2008a), which is able to simultaneously model the SED, the intensity images, and the JHK polarization images. Our model assumes a 2-D axis-symmetric disk surrounded by an envelope and a power law grain size distribution ($n \propto a^{-3.5}$ with the size a between 0.005 μm and a_{max} and different a_{max} values for the disk and envelope). We found that the CRL 2136 disk has a low mass of ~0.007 $M_\odot$, a large radius of ~2000 AU, a height of ~2000 AU at the outer boundary, an inclination angle of ~70°, and we estimated the disk accretion rate to be ~2.1 10^{-7} $M_\odot$ yr^{-1}. A small maximum grain size a_{max} of 0.45 μm is obtained for both the extended envelope and the disk. → Murakawa et al. 2008a, 2008b, 2008c

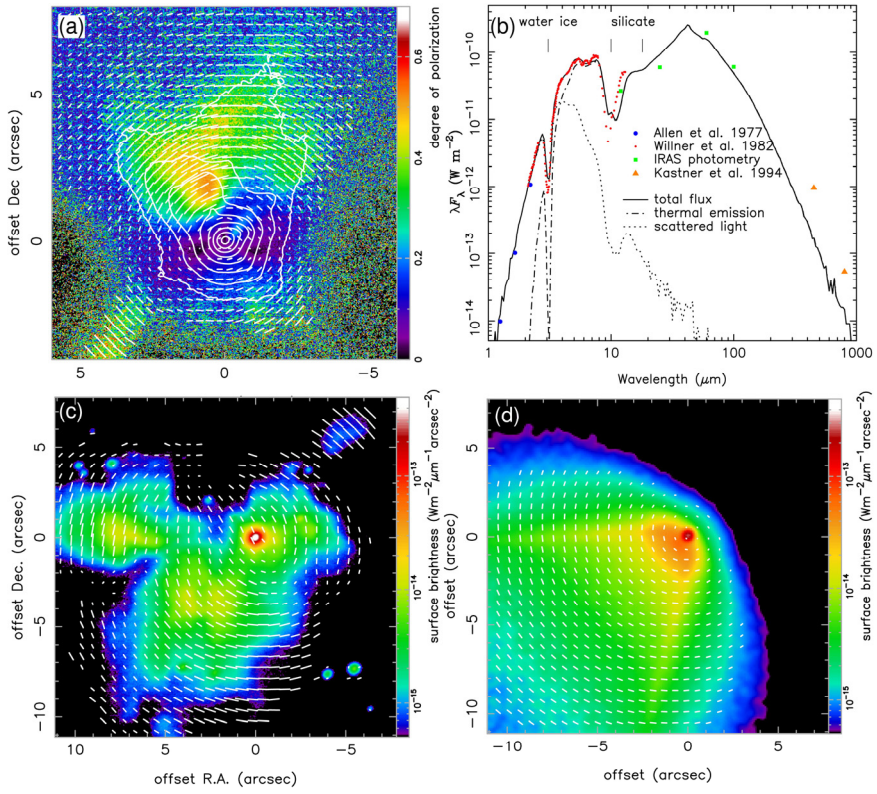

Figure 16: *(a) H-band degree-of-polarization image of R Mon overlaid with polarization vectors. The contour lines are the total intensity image. (b) Observed and model SEDs of CRL 2136. (c) K-band polarization image of CRL 2136 (intensity overlaid with polarization vectors). (d) 2-D radiative transfer model intensity image overlaid with model polarization vectors.*

STARS IN LATE EVOLUTIONARY STAGES

Spatially Resolving Inhomogeneous Structures of the Dynamical Atmosphere of the Red Supergiant Betelgeuse with VLTI/AMBER

Recent observations of RSGs from the UV to the radio reveal the co-existence of hot chromospheric plasma, molecular gas, and possibly even dust within several stellar radii. This inhomogeneous nature is a key to understanding the long-standing problem of mass loss in RSGs. Using VLTI/AMBER, we carried out spatially resolved, high spectral resolution ($\lambda/\Delta\lambda = 4800$–$12000$) observations of the CO first overtone lines between 2.28 and 2.31 μm for the RSG Betelgeuse (α Ori). Spectrally dispersed data were obtained in the second, third, and fifth visibility lobes (16, 32, and 48 m baselines, respectively), which represents the highest spatial resolution (9 mas) achieved for Betelgeuse at any wavelength from the UV to the radio (Figs. 17a–f). The visibilities and closure phases in the *continuum* can be reasonably fitted by a limb-darkened disk with a diameter of 43.56 ± 0.06 mas, showing little evidence of inhomogeneities. However, the AMBER data in the *CO lines* reveal salient inhomogeneous structures. The visibilities, differential phases, and closure phases within the individual CO lines show that the blue and red wings originate in spatially distinct regions over the stellar disk. Our AMBER data can be roughly explained by a simple "stellar patch" model with an inhomogeneous velocity field, in which a patch of the CO gas is moving outward with velocities of 10–15 km s^{-1}, while the CO gas in the remaining region is moving in the opposite direction (solid lines in Figs. 17a–f). This makes the star appear different in the blue and red wings (Fig. 17, bottom panels). These AMBER observations are the first to spatially resolve the so-called macroturbulence in a stellar photosphere other than the Sun. → Ohnaka et al. 2009, PR 2009

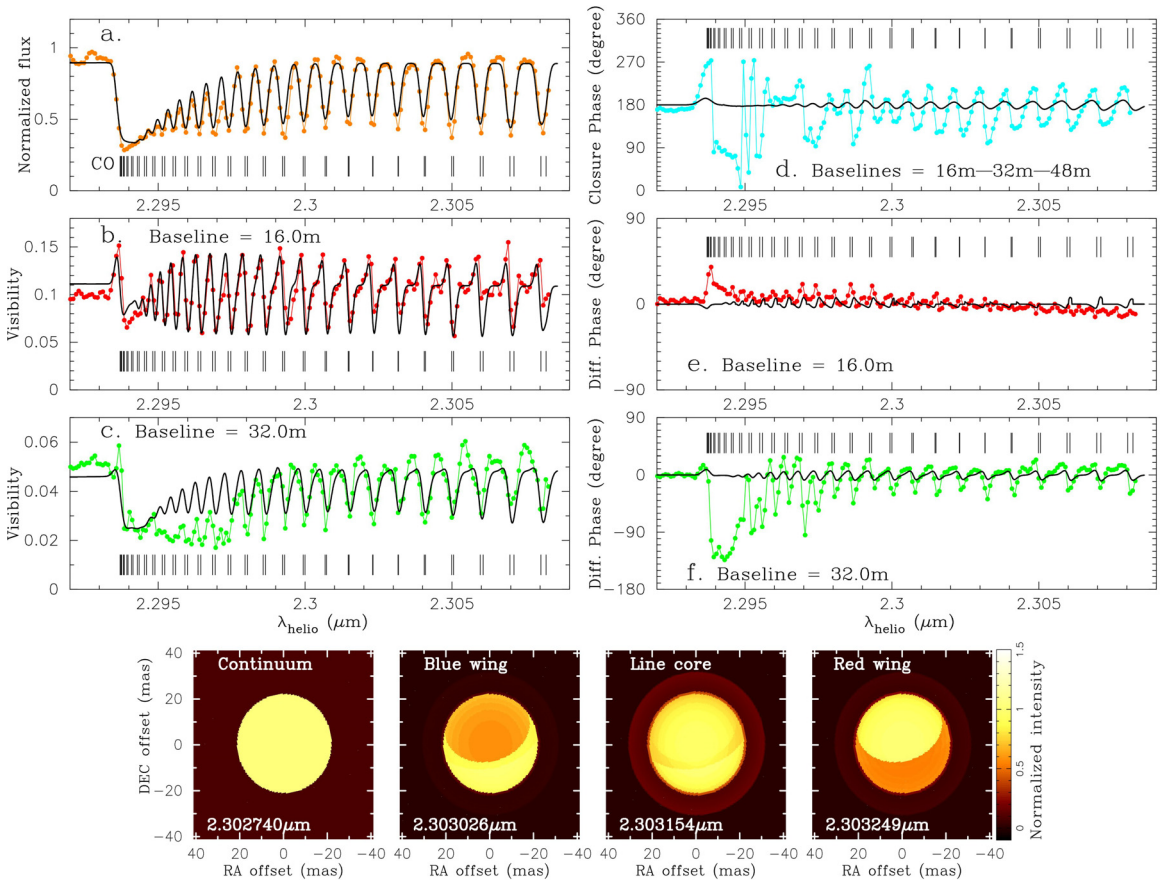

Figure 17: *AMBER observations of Betelgeuse compared with our stellar patch model. The observed spectrum (a), visibilities (b and c), closure phase (d), and differential phases (e and f) are plotted with dots, while the model is shown by solid lines. The positions of the CO lines are marked by the ticks. The bottom panels show the model images at four wavelengths within one CO line.*

Resolving the Asymmetric Inner Wind Region of the Yellow Hypergiant IRC+10420 with VLTI/AMBER in Low and High Spectral Resolution Mode

IRC+10420 is a massive evolved star belonging to the rare group of yellow hypergiants. Currently, this star is rapidly evolving through the Hertzprung-Russell diagram across the so-called yellow void. IRC+10420 is suffering from intensive mass loss, which led to the formation of an extended dust shell. Moreover, the dense stellar wind is subject to strong line emission.

We obtained AMBER observations of IRC+10420 in low spectral resolution (LR) mode in the *JHK* bands and in high spectral resolution (HR) mode around the Br γ-emission line (Fig. 18). In the HR observations, the visibilities show a noticeable drop across the Br γ line on all three baselines, and we detected wavelength-differential phases up to −25º in the redshifted part of Br γ and a non-zero closure phase close to the line center. From our LR data, we derived *FWHM* Gaussian sizes of 1.05 and 0.98 mas for IRC+10420's continuum-emitting region in the H and K bands, respectively. The Br γ-emitting region can be fitted with a geometric ring model with a diameter of 4.18 mas, which is approximately 4 times the stellar size. This model also provides evidence that the Br γ-emitting region is elongated towards a PA of 36º, well aligned with the symmetry axis of the outer reflection nebula.

The HR observations of IRC+10420 were further analyzed by means of gas radiative transfer modeling using the 1-D code CMFGEN (e.g., Hillier & Miller 1998) and its 2-D extension (Busche & Hillier 2005). Assuming an unclumped wind and a luminosity of $6\times10^5\ L_\odot$, the spherical CMGFEN modeling yields a current mass-loss rate of $1.5–2.0\times10^{-5}\ M_\odot \mathrm{yr}^{-1}$ based on the Br γ equivalent width. However, the spherical model poorly reproduces the observed line shape, blueshift, and extension, definitively showing that the IRC+10420 outflow is asymmetric. On the other hand, our 2-D radiative transfer modeling shows that the blueshifted Br γ emission and the shape of the visibility across the emission line can be explained with an asymmetric bipolar outflow with a high density contrast from pole to equator, where the redshifted light is substantially diminished. → Driebe et al. 2009

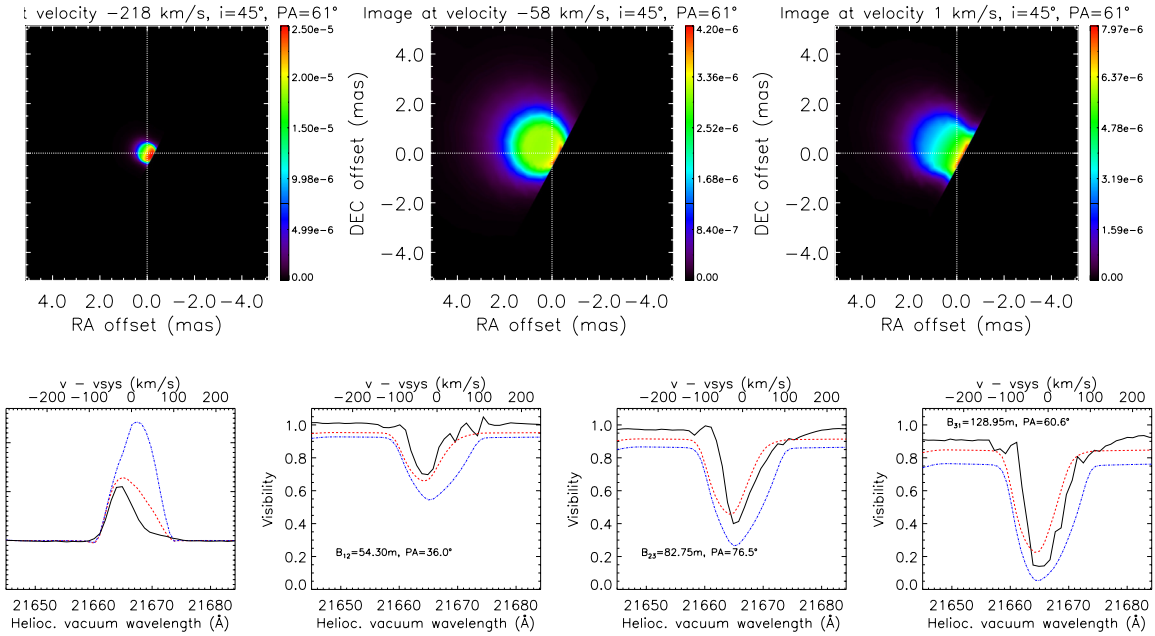

Figure 18: *Top row: Monochromatic images of IRC+10420 predicted by our 2-D radiative transfer model where the light from the southwestern redshifted lobe is blocked. From left to right, the panels show images in the K-band continuum (at a velocity of −218 km/s, i.e. well outside the line), the blueshifted Br γ emission at v = −58 km/s, and the center of the Br γ emission. Bottom row: Continuum-normalized AMBER spectrum (left) and visibilities (solid black line) around Br γ compared to our radiative transfer models without any blocking (blue) and with the redshifted part of the emission blocked (red; see top row). Note that the model with the blocked redshifted lobe can reproduce the observed Br γ flux and blueshift as well as the size of the emission region.*

Resolving the Dusty Torus of the Red Supergiant WOH G64: First VLTI Observations of an Individual Star in the *Large Magellanic Cloud*

Despite their importance in the chemical enrichment of galaxies, the evolution of massive stars ($\geq$8 $M_\odot$) is not well understood. Red supergiants (RSGs) in the Large Magellanic Cloud (LMC) provide an excellent opportunity to test the stellar evolution theory observationally, because the distance is well determined (50 kpc). WOH G64, the brightest RSG in the *LMC* in the mid-IR, challenges the evolution theory, since its position on the H-R diagram, based on the previously estimated luminosity, seriously disagrees with the theoretical evolutionary track (Fig. 19a). To tackle this problem, we spatially resolved its dust envelope in the N band with VLTI/MIDI − the first VLTI observations to resolve an individual star outside our Milky Way Galaxy. The visibilities measured at approximately the same baseline length show no noticeable dependence on position angle within the error bars (Fig. 19c). Our 2-D radiative transfer modeling demonstrates that the observed *N*-band visibilities and spectral energy distribution can be reproduced by an optically and geometrically thick silicate torus model viewed close to pole-on (Figs. 19b-e). The newly derived luminosity from our 2-D modeling, which is lower than the previous estimates based on spherical models by a factor of 2, brings the location of WOH G64 on the H-R diagram in much better agreement with a theoretical evolutionary track for a 25 $M_\odot$ star (Fig. 19a), supporting the current evolution theory. However, the low temperature of WOH G64 places it very close to or even beyond the Hayashi limit, implying that the star is possibly experiencing unstable, violent mass loss. → Ohnaka et al. 2008a; PR 2009

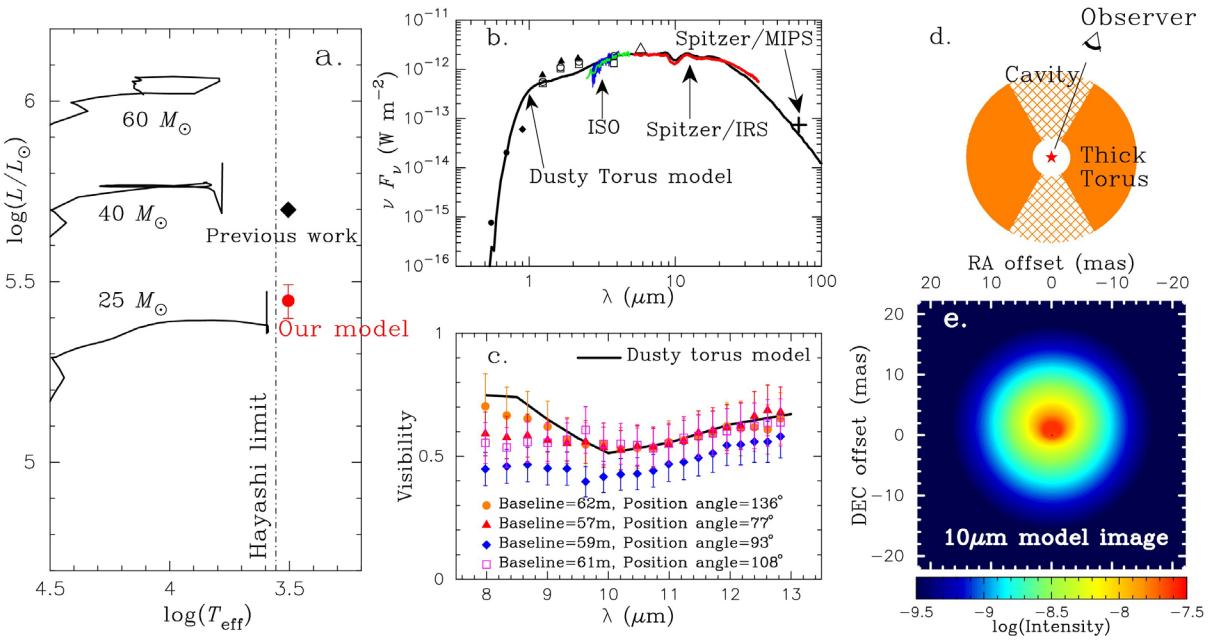

Figure 19: *2-D radiative transfer modeling of WOH G64. (a) Comparison between the observationally derived positions of WOH G64 (filled diamond and circle) and theoretical evolutionary tracks (solid lines, from Schaerer et al. 1993). (b) Observed SED (ground-based photometric data plotted with different symbols as well as ISO and Spitzer spectra) and the prediction of our dusty torus RT model (solid line). (c) Observed and model N-band visibilities. (d) Schematic view of the torus model. (e) 10 μm model image.*

Detection of Circum-Companion Disks Around Silicate Carbon Stars with VLBA and VLTI/MIDI

Silicate carbon stars possess O-rich circumstellar material, despite their C-rich photospheres. It is believed that the O-rich material shed by the past mass loss may be stored in circumbinary or circum-companion disks. While our previous MIDI observations of the silicate carbon star IRAS 08002-3803 suggested the presence of an optically thick circumbinary disk (Ohnaka et al. 2006), our recent VLBA images of the 22 GHz H_2O masers in the silicate carbon star EU And can be best interpreted as an edge-on circum-companion disk (Fig. 20, left) for the following reason. The mid-IR spectrum of EU And from the Spitzer archive data indicates that the dust emission is optically thin. If the disk were

circumbinary, the intense radiation pressure of the primary AGB star would blow away such an optically thin disk in a short period of time. The weak radiation pressure of the low-luminosity companion allows the disk to exist stably. Furthermore, our MIDI observations of BM Gem reveal strong non-zero differential phases in the 10 μm silicate feature (Fig. 20, middle), which represents a photocenter shift (see Fig. 20, right). The data can be explained by a model of a circum-companion disk with a trailing tail due to the orbital motion, which resembles an asymmetric ring or spiral (Fig. 20, right). These results support the presence of the long-sought circumbinary and circum-companion disks in silicate carbon stars. → Ohnaka et al. 2008b, 2008c

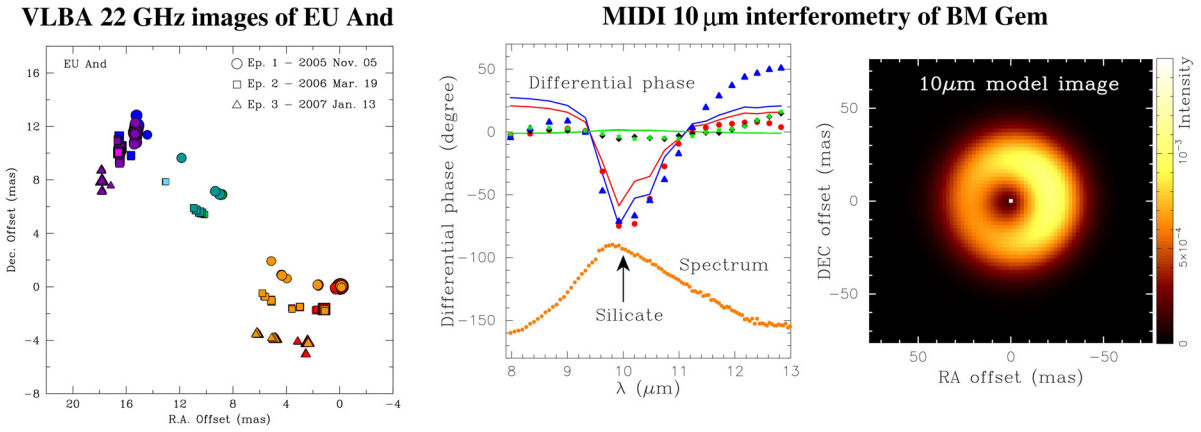

Figure 20: *Left: VLBA observations of EU And with the velocity of each maser spot color-coded (from red with $V_{LSR} = -33$ km s^{-1} to purple with $V_{LSR} = -43$ km s^{-1}). The size of the spot represents the maser flux density. Middle: Differential phases observed for BM Gem (symbols) and our model (solid lines with the colors corresponding to the data). The observed spectrum is shown by the orange dots. Right: 10 μm model image.*

VLTI/AMBER Spectro-Interferometric Aperture-Synthesis Imaging of VX Sgr's Inhomogenous Outer Atmosphere in the *H* and *K* Bands

We obtained VLTI/AMBER measurements of the cool, semi-regular M-type giant VX Sgr in the H and K bands (between 1.45 and 2.50 μm) to probe its upper photosphere and inner circumstellar environment and to shed more light on the open question whether VX Sgr is a red supergiant or an AGB star. The uv coverage allowed us to reconstruct images of VX Sgr for several wavelength channels (see Fig. 21). The spectro-interferometric data were also fitted to simple geometrical models and compared to the predictions of 1-D dynamical model atmospheres of Mira stars (Ireland et al. 2004) and to 3-D hydrodynamical calculations of a red supergiant (e.g., Freytag & Höfner 2008).
The reconstructed images (Fig. 21) and visibilities of VX Sgr show a strong wavelength dependence. The H-band images display two bright spots, whose positions are confirmed by the geometrical model fits. Such inhomogeneities are qualitatively predicted by 3-D simulations of the surface convection pattern of cool supergiants. At approximately 2.00 μm and in the region 2.35−2.50 μm, the photosphere appears extended and the apparent size is larger than in the H band. The wavelength dependence of the visibility across the H and K bands can be qualitatively explained by 1-D dynamical models of Mira atmospheres. In particular, H_2O seems to be the dominant absorber in VX Sgr's molecular layers. The best-fitting photospheric Mira models show a good match with the observed visibilities and give a photospheric diameter of 8.82 ± 0.50 mas. On the other hand, our comparison of the wavelength-dependent AMBER visibilities with the predictions of the hydrodynamical simulations of a supergiant are less satisfactory. VX Sgr's outer atmosphere is better represented by a model atmosphere of a Mira star than a red supergiant. → Chiavassa et al. 2010, arXiv:0911.4422v2

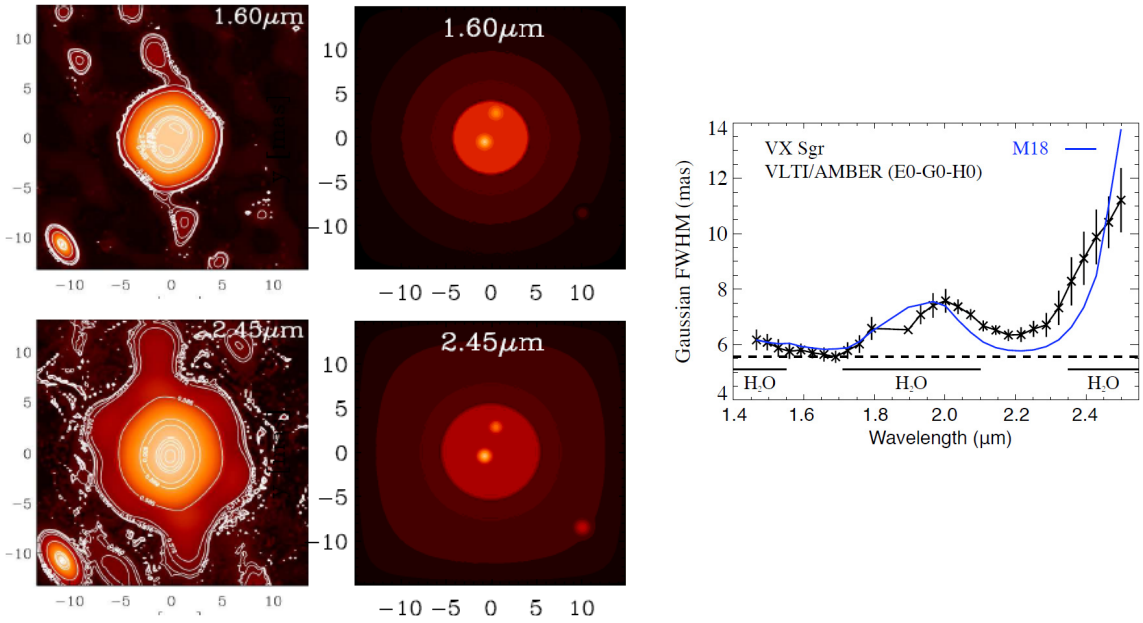

Figure 21: *Left: Reconstructed images with contour lines (left) and best-fitting geometrical models (right) of VX Sgr for two different wavelengths of our AMBER observations. All scales are in mas, and the resolution (beam) of the interferometer is illustrated in the bottom left part of each image. In the H band (top panels), two central spots are visible in both the reconstructed image and the best-fitting geometrical model. These spots can be associated with surface inhomogenities triggered by large-scale convection. Right: VX Sgr's Gaussian FWHM diameter derived from the AMBER observations as a function of wavelength, compared to the predictions of the dynamical Mira-star model M18 from Ireland et al. (2004).*

VLTI/AMBER Aperture-Synthesis Imaging of the B[e] Star HD 87643

HD 87643 is exhibiting the B[e] phenomenon; i.e., it is a B-type star whose spectrum contains permitted and forbidden emission. It is surrounded by large amounts of dust, detected by its strong infrared excess. We observed HD 87643 with the near-IR AMBER and the mid-IR MIDI VLTI instruments, the NACO/VLT AO instrument, and the ESO 2.2 m optical Wide-Field Imager. Our goal was to resolve the dust environment of HD 87643. The obtained AMBER/VLTI visibilities and closure phases show strong modulations and were used to reconstruct H- and K-band aperture-synthesis images of HD 87643 (fig. 22). These images are among the first few images reconstructed from VLTI data, together with the image of the young, high-mass binary θ^1 Ori C (Kraus et al. 2009), the Mira star T Lep (Le Bouquin et al. 2009), and the yellow hypergiant star VX Sgr (Chiavassa et al. 2009). The HD 87643 images show a northern companion at a separation of 34 mas and an extended shell around the primary star. The SED of the primary shell, the companion, and the circumbinary envelope were determined. A binary orbit with high eccentricity and periodic, violent mass ejections during previous periastron passages are possibly the keys to interpreting the extreme characteristics of this system. → Millour et al. 2009b

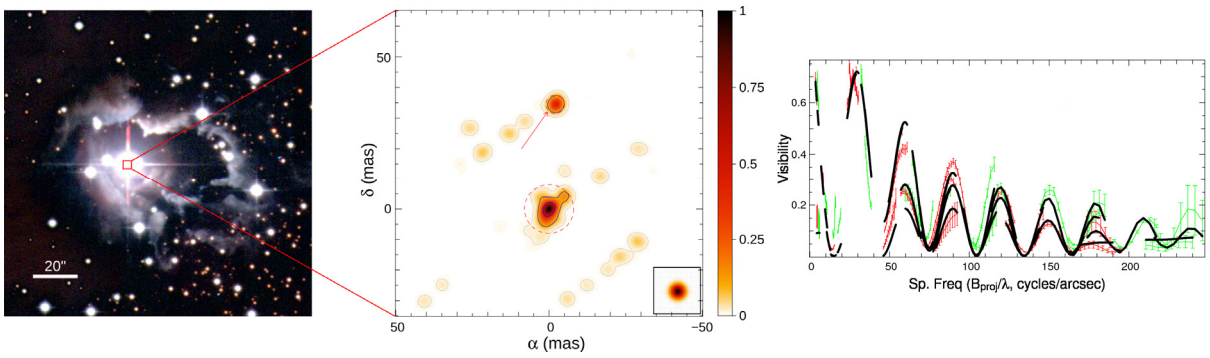

Figure 22: *Left: WFI image showing the reflection nebula. Middle: K-band aperture-synthesis image of HD 87643. Right: Visibilities (observations: green and red; model: black lines)*

VLTI/AMBER Near-Infrared Interferometry of the Dust-Forming Nova V1280 Sco During its 2007 Outburst

The images of several novae show complex bipolar shapes that currently cannot be explained well. Therefore, it is important to probe if this complex structure is already present in the early phases of the outburst to better understand the mechanisms that trigger nova outbursts. We obtained the first high spatial resolution monitoring of a nova in the infrared by observing the dust-forming nova V1280 Sco with the VLTI. These observations aim at improving the distance determination and constraining the mechanisms leading to very efficient dust formation under the harsh physical conditions encountered in nova ejecta. Spectra and visibilities were regularly obtained from the onset of the dust formation 23 days after discovery (or 11 days after maximum) until day 145 using AMBER (near-IR) and MIDI (mid-IR). Geometrical models and spherical dust shell models generated with the DUSTY radiative transfer code were used to model the dust shell. These observations allow us to determine an apparent linear expansion rate for the dust shell of 0.35 ± 0.03 mas/day and the approximate time of dust formation. This information, combined with the spectroscopically determined expansion velocity of 500 ± 100 km/s, implies a distance of 1.6 ± 0.4 kpc. The sparse uv coverage does not allow us to get clear indications of deviation from spherical symmetry. Dust envelope parameters could be determined with the 1-D DUSTY code. The dust mass generated was ~2−8 10^{-9} $M_{\odot}$/day, with a probable peak in dust production about 20 days after the detection of dust and another peak after 110 days, when the amount of dust in the shell was estimated to be 2.2 10^{-7} $M_{\odot}$. → Chesneau et al. 2008

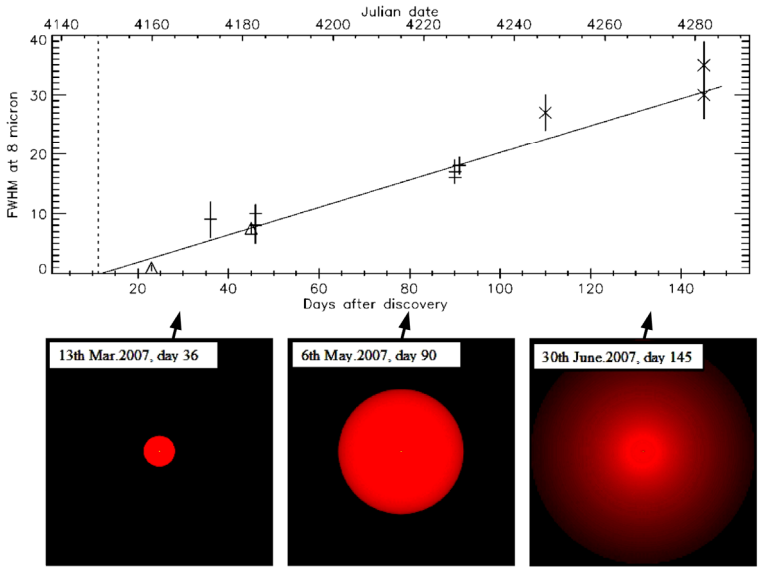

Figure 23: *Top: VLTI/AMBER (triangles) and VLTI/MIDI (crosses) measurements of the UD diameters of the nova V1280 Sco fireball as a function of time. One can clearly see its expansion at a rate of 0.35 ± 0.03 mas/day. Bottom: DUSTY model images at the different dates of observation.*

Is the Wolf-Rayet Star WR 118 Surrounded by a Pinwheel Nebula?

Wolf-Rayet stars (WR) are massive evolved stars, whose fate is to explode as supernovae. Most WR stars of the WC9 subtype exhibit a dusty circumstellar envelope, but it is still a matter of debate how dust can form in their hostile environment. In some cases, a pinwheel-like structure of the dusty envelope was detected. It has been suggested that dust formation in all dusty WR stars might be caused by colliding winds in a binary system.

Using ESO's VLTI/AMBER instrument with spectral resolution 35, we investigated the spatial structure of the innermost circumstellar dust shell of the deeply embedded WR star WR 118. The K-band observations were obtained with three 1.8 m telescopes, spanning projected baselines between 9 and 40 m. The measured closure-phase signal clearly shows that the circumstellar envelope of WR 118 is asymmetric. We showed that a pinwheel nebula seen at low inclination is consistent with the AMBER data (Fig. 24). The size and outflow opening angle of the best-fit pinwheel model were 14 mas and 58°, respectively. → Millour et al. 2009a

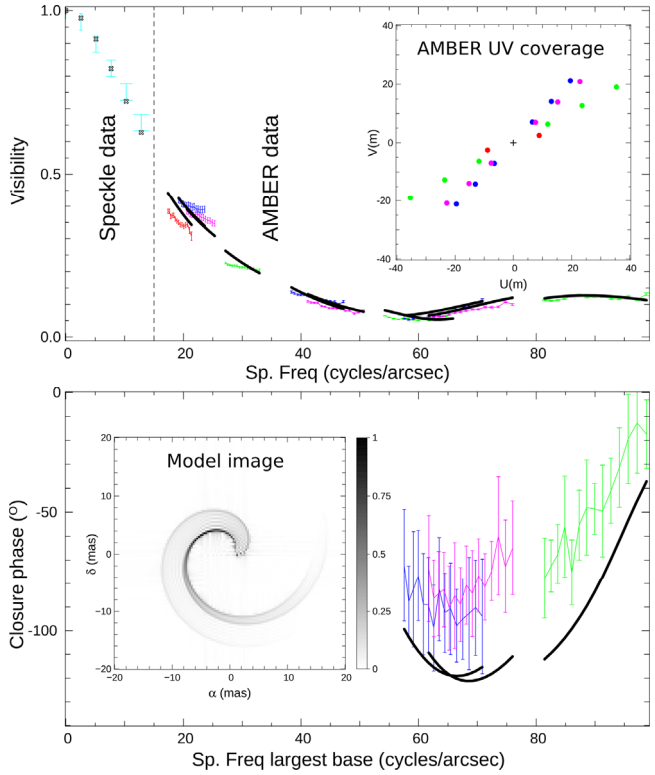

Figure 24: *Top: Observed visibilities (small blue, green, and red symbols) compared to our best-fit pinwheel model (black lines, the inset shows the VLTI UV coverage). Bottom: Observed closure phases (blue, green, and red vertical lines) compared to the same best-fit model (black lines, the inset shows the best-fit model image).*

MIDI and AMBER Interferometry of Classical Be Stars

Classical Be stars are hot non-supergiant stars that are surrounded by a gaseous circumstellar environment whose formation, geometry, and kinematics are still highly debated. The study of the mass-loss of these objects is crucial to progress in the understanding of the evolution of B stars. We carried out a survey of the brightest southern Be stars using the VLTI and its instruments MIDI and AMBER. Two of the resolved stars are α Ara and κ CMa. Modeling the spectro-interferometric measurements using the large-velocity-gradient-approximation-based radiative transfer code SIMECA for gaseous envelopes (Stee et al. 1995), we found that α Ara is a quasi-critical rotator surrounded by a Keplerian rotating equatorial disk and an enhanced polar wind, while κ CMa is rotating at only half the critical velocity and is surrounded by a sub-Keplerian rotating disk but shows no evidence of an enhanced polar wind. Effects of the stellar rotation can fully explain the ejection of matter in the case of α Ara. The centrifugal force almost fully compensates the gravity at the equator. This allows matter to escape easily from the stellar surface and to form a Keplerian rotating disc. The latitudinal dependence of the stellar effective gravity also causes the poles to be twice as hot as the equator, allowing the launching of the enhanced polar wind. → Meilland et al. 2008 and 2009

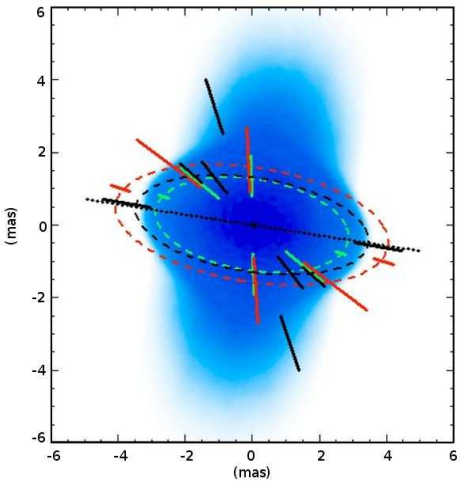

Figure 25: *VLTI/MIDI interferometry of α Ara at 8μm (green bars) and 12μm (red bars) assuming a uniform disk + unresolved star model as well as VLTI/AMBER measurements (black bars) and the corresponding best-fit SIMECA model in the continuum (blue intensity distribution). The black, green, and red ellipses correspond to the uniform-ellipse fit of the equatorial disk at 2.1, 8, and 12 μm, respectively. The orientation of the major axis (dotted black line) is perpendicular to the polarization angle measurement.*

Resolving the Circumstellar Envelope of the A[e] Supergiant HD 62623

A[e] and B[e] stars are hot stars surrounded by circumstellar gas and dust responsible for the presence of emission lines and IR excess in their spectra. How dust can form in the hot environment of these stars remains an open issue. Using the VLTI/MIDI instrument, we observed HD 62623, one of the very few A-type supergiants showing the B[e] phenomenon. We showed that the circumstellar environment is partially resolved even at the shortest baselines. We used two different radiative transfer codes to obtain a model of the N-band emission of the circumstellar environment of this peculiar star:
- MC3D (Wolf et al. 1999): a Monte-Carlo code for dusty circumstellar envelopes.
- SIMECA (Stee et al. 1995): a large-velocity-gradient-approximation code for gaseous environments.
The results of this modeling are summarized in Fig. 26. Most of the measurements are well fitted by a $2 \cdot 10^{-7}\,M_{\odot}$ dusty disk with an inclination angle of $60 \pm 10°$ and an inner radius of 3.9 ± 0.6 AU, corresponding to a sublimation temperature of about 1250 K. This is the first time that the dusty inner disc rim of a supergiant star exhibiting the B[e] phenomenon is significantly constrained. The larger baselines seem to indicate that 10−20% of the total N-band flux originates from a more compact structure, which is well modeled as the inner gaseous disk (blue inner region in the model image: Fig. 26 right). → Meilland et al., accepted; arXiv: 0912.1954

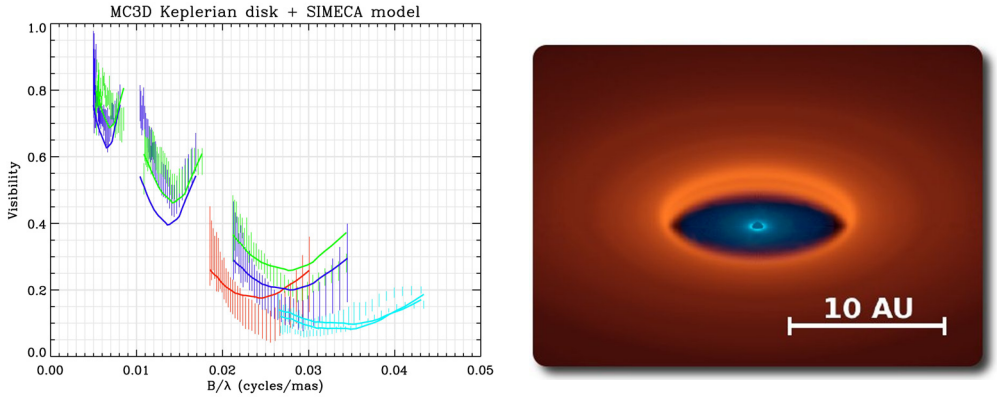

Figure 26: *Left: VLTI/MIDI mid-IR visibilities of HD 62623 plotted as a function of the spatial frequency for nine baselines. The measurements with their error bars are plotted as vertical lines. The best SIMECA + MC3D model curves are plotted as solid lines. Right: Corresponding SIMECA (blue) + MC3D (red) composite image of the best-fit model.*

The Quasi-WR Star HD 45166: Fundamental Stellar Parameters and Evidence for a Latitude-Dependent Wind

The enigmatic star HD 45166 is a quasi-WR (qWR) star in a binary system with an orbital period of 1.596 days. It presents a rich emission-line spectrum in addition to absorption lines from the companion star (B7V). Because the system inclination is very small (i = 0.77°), HD 45166 is an ideal laboratory for wind-structure studies. We determined the fundamental stellar and wind parameters of this qWR star, computing a radiative transfer model for the wind and photosphere with the non-LTE code CMFGEN (Hillier & Miller 1998). The wind asymmetry was also analyzed using a recently developed version of CMFGEN to compute the emerging spectrum in two-dimensional geometry. The qWR star has an effective temperature of $T_{\rm eff} = 50000 \pm 2000$ K, a luminosity of $\log(L/L_{\odot}) = 3.75 \pm 0.08$, and a corresponding photospheric radius of $R_{\rm eff} = 1.00\,R_{\odot}$. The star is helium-rich ($N_H/N_{He} = 2.0$), while the CNO abundances are anomalous when compared either to the Sun, to planetary nebulae, or to WR stars. The comparison between the observed line profiles and models computed under different latitude-dependent wind densities strongly suggests the presence of an oblate wind-density enhancement similar to a wind compression zone, since the equatorial wind is about 8 times denser than the polar wind (Fig. 27). → Groh et al. 2008

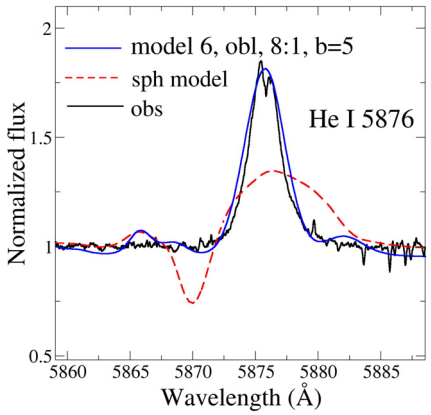

Figure 27: *Comparison of the line profiles computed with the 2-D code of Busche & Hillier (2005) (blue line) with the observations of HD 45166 around He I λ5876 (black line). The model is labeled with the equator/pole density contrast and the parameter b, which controls the shape of the density variation. The best spherical-symmetric CMFGEN model (dashed red line) is shown for comparison. The weak dip in the observed He I λ5876 line profile is likely due to incomplete subtraction of the secondary star spectrum.*

Near-Infrared Integral Field Spectroscopy of the Homunculus Nebula Around η Carinae Using Gemini/CIRPASS

We obtained the first integral field spectroscopy of the Homunculus and Little Homunculus nebulae around η Carinae in the near-infrared spectral region (J band). We confirmed the presence of a hole in the polar region of each lobe, as indicated by previous near-IR, long-slit spectra and mid-IR images. The holes can be described as a cylinder of height of 6.5×10^{16} cm and diameter of 6.0×10^{16} cm. We also mapped the blue-shifted component of He I λ10830 seen towards the NW lobe. Contrary to previous works, we suggested that this blue-shifted component is indeed in the equatorial disc. We showed that the spatial extent of the so-called Little Homunculus matches the radio continuum emission at 3 cm remarkably well, indicating that it can be regarded as a small H II region. Therefore, we used the optically thin 1.3 mm radio flux to derive a lower limit for the number of Lyman-continuum photons of the central source in η Car. In the context of a binary system, and assuming that the ionizing flux comes entirely from the hot companion star, the lower limit for its spectral type and luminosity class ranges from O5.5 III to O7 I. → Teodoro et al. 2008

On the Nature of the Prototype LBV AG Carinae: Fundamental Parameters During Visual Minimum Phases and Changes in the Bolometric Luminosity During the S-Dor Cycle

We analyzed the evolution of the luminous blue variable (LBV) AG Carinae during the last two visual minimum phases of its S-Dor cycle (1985–1990 and 2000–2003), employing state-of-the-art radiative transfer modeling with CMFGEN for the ultraviolet (Fig. 28), optical, and near-infrared spectrum of AG Car. We found that the minimum phases of AG Car are not equal to each other, since we derived a noticeable difference between the effective temperature achieved from 1985–1990 (22800 K) and 2000–2001 (17000 K). Significant differences between the wind parameters in these two epochs were also noticed. While the wind terminal velocity was 300 km/s from 1985–1990, it was as low as 105 km/s in 2001. The mass-loss rate, however, was lower from 1985–1990 (1.5×10^{-5} $M_\odot$/yr) than 2000–2001 (3.7×10^{-5} $M_\odot$/yr). We found that the wind of AG Car is significantly clumped ($f \simeq 0.10$–0.25) and that clumps must be formed deep in the wind. We derived a bolometric luminosity of 1.5×10^6 $L_\odot$ during both minimum phases which, contrary to the common assumption, decreases to 1.0×10^6 $L_\odot$ as the star moves toward the maximum flux in the V band. Assuming that the decrease in the bolometric luminosity of AG Car is due to the energy used to expand the outer layers of the star, we found that the expanding layers contain roughly 0.6−2 $M_\odot$. Such an amount of mass is an order of magnitude lower than the nebular mass around AG Car, but it is comparable to the nebular mass found around lower-luminosity LBVs and to that of the Little Homunculus of η Car. If such a large amount of mass is indeed involved in the S Dor-type variability, we speculate that such instability could be a failed Giant Eruption, with several solar masses never becoming unbound from the star. → Groh et al. 2009

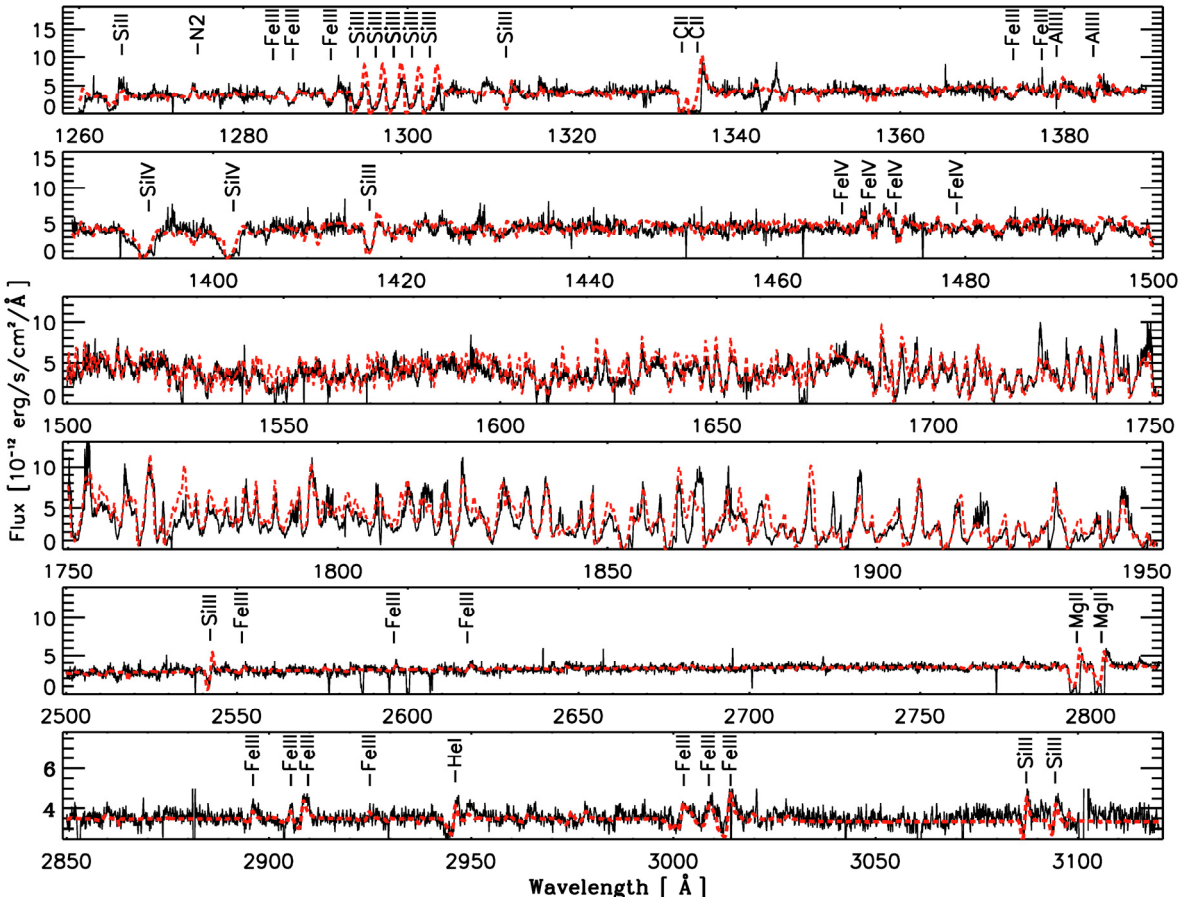

Figure 28: *Comparison between the ultraviolet spectrum of AG Car from 1989 Dec. 23 (solid black line) and the best CMFGEN model for that epoch reddened using E(B−V) = 0.65 and RV = 3.5 (dashed red line) in the spectral region between 1260–3150 Å. Line identification for the strongest spectral features is presented. The spectrum in the region between 1500 and 1950 Å is highly blanketed and dominated by blends of Fe III, Fe IV, and Ni IV lines. Note that Fe II lines are absent. The P III doublet lines at 1344.32–1344.85 Å were not included in the models.*

Bona-Fide, Strong-Variable Galactic Luminous Blue Variable Stars are fast Rotators: Detection of a High Rotational Velocity in HR Carinae

We obtained optical observations of the luminous blue variable (LBV) HR Carinae which show that the star reached a visual minimum phase in 2009. We detected absorptions due to SiIV λλ4088−4116. To match their observed line profiles from 2009 May, a high rotational velocity of $v_{rot} \simeq 150 \pm 20$ km/s is needed (assuming an inclination angle of 30°), implying that HR Car rotates at $\simeq 0.88 \pm 0.2$ of its critical velocity for breakup (v_{crit}). Our results suggest that fast rotation is typical in all strong-variable, bona-fide galactic LBVs which present S-Dor-type variability. Strong-variable LBVs are located in a well-defined region of the HR diagram during visual minimum (the "LBV minimum instability strip"). We suggest this region corresponds to the region where v_{crit} is reached (Fig. 29). To the left of this strip, a forbidden zone with $v_{rot}/v_{crit} > 1$ is present (Fig. 29), explaining why no LBVs are detected in this zone. Since dormant/ex LBVs like P Cygni and HD 168625 have low v_{rot}, we propose that LBVs can be separated into two groups: fast-rotating, strong-variable stars showing S-Dor cycles (such as AG Car and HR Car) and slow-rotating stars with much less variability (such as P Cygni and HD 168625). We speculate that supernova progenitors which had S-Dor cycles before exploding could have been fast rotators. We suggest that the potential difficulty of fast-rotating Galactic LBVs to lose angular momentum is additional evidence that such stars could explode during the LBV phase. → Groh et al. 2009

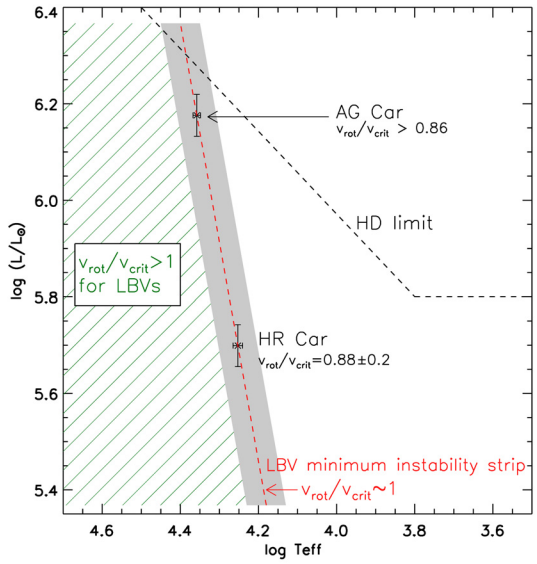

Figure 29: *HR diagram showing the position of the strong-variable LBVs AG Car and HR Car during visual minimum, according to the updated stellar parameters determined in this work. A revised position for the LBV minimum instability strip is derived (dashed red line) and is considerably steeper than previous determinations (Wolf 1989; van Genderen 2001; Clark et al. 2005). Notice that AG Car and HR Car are both fast rotators during minimum, which suggests that the LBV minimum instability strip corresponds to the location where critical rotation is reached for strong-variable LBVs. The location of the Humphreys–Davidson limit (Humphreys & Davidson 1994) is shown (dashed black line).*

Probing the Circumstellar Environment of the AGB Star π^1 Gru with VLTI/MIDI

The formation of complex structures seen in planetary nebulae from spherically symmetric circumstellar envelopes at the AGB is one of the major problems in stellar astrophysics. Using MIDI, we studied the circumstellar environment of the AGB star π^1 Gru, for which bipolar outflows are detected by arcsec-scale mm-observations. The MIDI data show no significant deviation from spherical symmetry in the innermost region of the circumstellar environment and can be explained by a warm molecular layer extending to ~4 stellar radii and an optically thin dust shell consisting of silicate and Al_2O_3 with an inner boundary radius of 14 stellar radii . → Sacuto et al. 2008

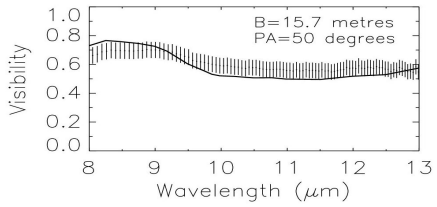

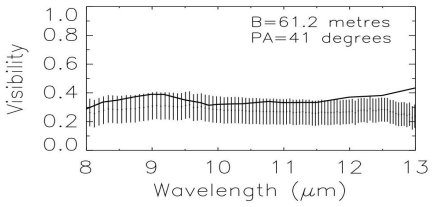

Figure 30: *MIDI data (dots with error bars) and our model with a warm molecular layer and a dust shell (solid lines) for π^1 Gru.*

JHK Spectro-Interferometry of the Mira Star S Ori with VLTI/AMBER

Understanding the physical properties of the outer atmosphere of Mira stars is of vital importance for obtaining insights into the mass-loss mechanism in AGB stars. Our *JHK* AMBER observations (1.3−2.3 μm) of S Ori have revealed that the angular size of the star is significantly affected by the H_2O and CO bands. The angular diameters in these molecular bands are 25−50% larger than those at near-continuum wavelengths. The observations are reasonably well reproduced by the dynamical model atmosphere of Ireland et al. (2004). The larger size in the molecular bands is explained by the formation of molecular shells behind shock fronts propagating outward. → Wittkowski et al. 2008

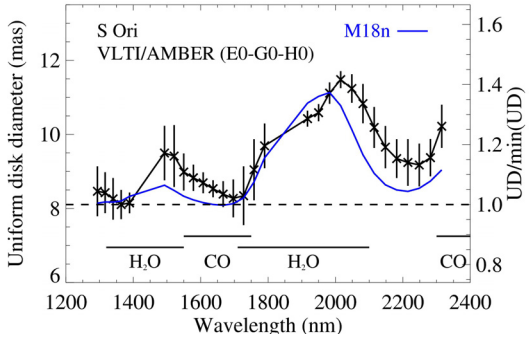

Figure 31: *Uniform disk diameter of S Ori measured with AMBER using the E0-G0-H0 (16-32-48 m) baselines (crosses) and the one predicted by the dynamical model (blue line) of Ireland et al. (2004).*

People involved: T. Beckert, L. Chen, T. Driebe, J. Groh, K.-H. Hofmann, S. Hönig, M. Kishimoto, S. Kraus, A. Liermann, A. Meilland, F. Millour, K. Murakawa, N. Nardetto, K. Ohnaka, Th. Preibisch, D. Schertl, K. Tristram, G. Weigelt

Collaborators:
K. Agabi (Univ. Nice), N. Ageorges (ESO), P. Antonelli (Obs. de la Côte d'Azur), R. Antonucci (Univ. of California), F. Bacciotti (INAF), C. Baffa (Arcetri Obs.), I.I. Balega (Special Astrophysical Obs.), Y.Y. Balega (Special Astrophysical Obs.), R. Barvainis (NSF), M. Benisty (Univ. Grenoble), J.-P. Berger (Univ. Grenoble), J.-L. Beuzit (Univ. Grenoble), D. Boboltz (US Naval Obs.), A. Boden (CalTech), D. Bonneau (Univ. Nice), L. Burtscher (MPIA), A. Chelli (Univ. Grenoble), O. Chesneau (Obs. de la Côte d'Azur), P. Cruzalèbes (Obs. de la Côte d'Azur), A. Damineli (Univ. de São Paulo), W.J. de Witt (Univ. Grenoble), E. di Folco (Obs. de Genève), J.A. Docobo (Univ. of Santiago de Compostela), A. Domiciano de Souza (Univ. Nice), M. Duget (Obs. de la Côte d'Azur), W.J. Duschl (Univ. Kiel), G. Duvert (Univ. Grenoble), A. Eckart (Univ. of Cologne), M. Elitzur (Univ. Kentucky), T. Forveille (Lab. d'Astrophysique de Grenoble), R. Foy (Univ. Lyon), D. Fraix-Burnet (Univ. Grenoble), P. Gandhi (Cambridge Univ.), C. Gil (ESO), D. Gillet (Obs. de Haute-Provence), R. Gilli (INAF), A. Glindemann (ESO), L. Glück (Univ. Grenoble), K.N. Grankin (Crimean Astrophysical Obs.), U. Graser (MPIA), V. Grinin (Pulkovo Obs.), A. Gross (MPIA), Th. Henning (MPIA), G.H. Herbig (Univ. Hawaii), T. Herbst (MPIA), D.J. Hillier (Univ. Pittsburgh), H. Horst (Univ. Kiel), C.A. Hummel (ESO), E.M.L. Humphreys (Harvard-Smithsonian Center for Astrophysics), N. Ikhsanov (Univ. Cambridge), A. Isella (Arcetri Obs.), W. Jaffe (Sterrewacht Leiden), P. Kervella (LESIA), M. Kiekebusch (ESO), V.G. Klochkova (Special Astrophysical Obs.), T. Kotani (ISAS), S. Lagarde (Obs. de la Côte d'Azur), J.-B. le Bouquin (ESO), E. Le Coarer (Univ. Grenoble), Ch. Leinert (MPIA), G. Li Causi (OAR), F. Lisi (Arcetri Obs.), B. Lopez (Obs. de la Côte d'Azur), A.F. Maksimov (SAO), F. Malbet (Univ. Grenoble), E.V. Malogolovets (SAO), E. Mamajek (Harvard-Smithsonian Center for Astrophysics), A. Marconi (Univ. Florence), F. Massi (INAF), P. Mathias (Obs. de la Côte d'Azur), K. Meisenheimer (MPIA), F. Ménard (Lab. d'Astrophysique de Grenoble), S. Mensh'chikov (Inst. for Comput. Astrophysics, Halifax), A. Merand (ESO), M. Meyer (Steward Obs.), R. Millan-Gabet (CalTech), M. Min (Sterrenkundig Inst. Anton Pannekoek), A.S. Miroshnichenko (Univ. of North Carolina), J.-L.Monin (Univ. Grenoble), J.D. Monnier (Univ. Michigan), D. Mourard (Obs. de la Côte d'Azur), G.C. Murphy (Lab. d'Astrophysique de Grenoble), A. Natta (Osservatorio Astrofisico di Arcetri), J. Nishikawa (NAO Japan), S. Oya (NAO Japan), E. Pedretti (Univ. Michigan), K. Perraut (Univ. Grenoble), C. Perrier (Univ. Grenoble), G. Perrin (LESIA), M. Petr-Gotzens (ESO), R. Petrov (Univ. Nice), M. Polletta (IAP, Paris), J.U. Pott (WMKO) A.M. Prieto (MPIA), P. Puget (Univ. Grenoble), A. Quirrenbach (ZAH Landessternwarte), D. Raban (Sterrewacht Leiden), Y. Rabbia (Obs. de la Côte d'Azur), F. Rantakyrö (ESO), A. Richichi (ESO), S. Robbe-Dubois (Univ. Nice), C. Rossi (Università di Roma), H. Röttgering (Sterrewacht Leiden), S. Sacuto (UMR 6525), P. Salinari (Arcetri Obs.), F.P. Schloerb (Univ. Massachussets), R. Schödel (IAA), D. Ségransan (Obs. de Genève), M. Schöller (ESO), M. Scholz (Univ. Heidelberg), Z. U. Shkhagosheva (SAO), A. Smette (ESO), M.D. Smith (Armagh Obs.), P. Stee (Obs. de la Côte d'Azur), J. Storm (Astrophys. Inst. Potsdam), V.S. Tamazian (Univ. of Santiago de Compostela), L.V. Tambovtseva (Pulkovo Obs.), E. Tatulli (Univ. Grenoble), M. Teodoro (Univ. de São Paulo), L. Testi (ESO), E. Thiébaut (Univ. Lyon), W.A. Traub (Harvard-Smithsonian Center for Astrophysics), P. Tuthill (Univ. Sydney), F. Vakili (Univ. Nice), R. van Boekel (MPIA), M. Vannier (Univ. Nice), B. Vollmer (Univ. Strasbourg), L.B.F.M. Waters (Astron. Inst. Anton Pannekoek), D. Weedman (Cornell Univ.), P.A. Whitelock (South African Astron. Obs.), M. Wittkowski (ESO), J. Woillez (WMKO), P.R. Wood (Australian Nat. Univ.), J. Young (Univ. of Cambridge), H. Zinnecker (AIP), G. Zins (Univ. Grenoble).